Towards scale-up of graphene production via non-oxidizing liquid exfoliation methods

Jason Stafford*, Andrius Patapas, Nwachukwu Uzo, Omar K. Matar, and Camille Petit

Department of Chemical Engineering, Imperial College London, SW7 2AZ, UK

*Corresponding author: j.stafford@imperial.ac.uk

Corresponding author: camille.petit@imperial.ac.uk

Abstract

Graphene, the two-dimensional form of carbon, has received a great deal of attention across academia and industry due to its extraordinary electrical, mechanical, thermal, chemical, and optical properties. In view of the potential impact of graphene on numerous and diverse applications in electronics, novel materials, energy, transport, and healthcare, large-scale graphene production is a challenge that must be addressed. In the past decade, top-down production has demonstrated high potential for scale-up. This review features the recent progress made in top-down production methods that have been proposed for the manufacturing of graphene-based products. Fabrication methods such as liquid-phase mechanical, chemical and electrochemical exfoliation of graphite are outlined, with a particular focus on non-oxidizing routes for graphene production. Analysis of exfoliation mechanisms, solvent considerations, key advantages and issues, and important production characteristics including production rate and yield, where applicable, are outlined. Future challenges and opportunities in graphene production are also highlighted.

Keywords: Graphene, Large-scale, Production, Exfoliation, 2D materials.

Table of Contents

1. Introduction 9

2. Publications and patents 11

3. Graphene-based materials 12

4. Existing production routes 13

5. Liquid-phase exfoliation 15

5.1 Precursor 15

5.2 Graphene dispersion 19

5.2.1 Solvents 19

5.2.2 Surfactants 23

5.2.3 Reductive dissolution 26

5.3 Exfoliation mechanisms 27

5.3.1 Mechanical exfoliation 28

5.3.2 Chemical exfoliation 28

5.3.3 Electrochemical exfoliation 31

5.4 Exfoliation methods 31

5.4.1 Solvothermal route 32

5.4.2 Microwave irradiation 34

5.4.3 Supercritical Fluids 37

5.4.4 Vortex fluidic device 38

5.4.5 Taylor-Couette device 40

5.4.6 Spinning disc processor 41

5.4.7 High-shear mixing 42

5.4.8 Sonication 45

5.4.9 Jet cavitation 47

5.4.10 Chaotic flow with sonication 48

5.4.11 Electrochemical exfoliation 49

Anodic Exfoliation 50

Cathodic Exfoliation 51

Shear-assisted electrochemical exfoliation 52

6. Challenges and Outlook 53

6.1 Control and characterisation of material properties 54

6.2 Solvents 55

6.3 Rheology 56

6.4 Integration with chemical engineering processes 57

6.5 Modelling and simulation 58

6.6 Other 2D materials 59

7. Conclusions 59

8. Acknowledgement 65

9. List of abbreviations 65

10. References 66

List of Figures

Figure 1: Publications and Patents in the field of graphene and graphene production. a) Number of publications on Graphene and Graphene Production from 2000 to 2016. This information was sourced from ISI Web of science. Search criteria for both are: Topic= "Graphene" and Topic= "Graphene" and "Production" respectively. b) Number of patents on Graphene and Graphene production from 2000 to 2016. This information was sourced through a worldwide search using the European Patent Offices Espacenet database. Search criteria for both are: Title and Abstract= "Graphene" and Title and Abstract= "Graphene" and "Production" respectively. Data for 2016 is incomplete and lower than expected as there is a typical timeline between filing and publication. 83

Figure 2: The trends in number of publications for Graphene and Graphene Production topics between 2000 and 2016. Data taken from Figure 1 a). 84

Figure 3: Overview of graphite and the various types of graphene-based materials with corresponding representative microscopy images. a) Scanning Electron Microscopy (SEM) image of expanded highly orientated pyrolytic graphite from Cooper *et al*. (b - c) TEM images of mono- and multi-layer graphene from Qian *et al*. d) SEM image of GO from Voiry *et al*. e) High resolution TEM (HRTEM) image of single layer reduced graphene oxide with indications of holes (red arrow) and oxygen functional groups (blue arrow) from Voiry *et al*. Reproduced with permission from ref. [53], [26] and [130]. Copyright 2014 Elsevier B.V., Copyright 2009 Springer, Copyright 2016 American Association for the Advancement of Science. 85

Figure 4: Top-down and bottom-up routes to graphene production. The intrinsic relationship between production (also reduction) approaches and graphene-based material type is also shown. 86

Figure 5: Summary of graphene production methods [16-29] . Criteria for data selection: a method results in at least 50% production of graphene with ≤5 layers, and has reported values for yield (wt%) and production rate (g/h).....87

Figure 6: Summary of the graphite precursor considerations and effects on graphene production...88

Figure 7: a) Hansen space representation and b) surface tension plot of solvents used for exfoliation and dispersion of graphene. Experimental data from [62].....89
Figure 8: a) Comparison between the potential of mean force for NMP, predicted by MD simulations of two graphene monolayers [66], and the classical Lennard-Jones (van der Waals) interaction potential in vacuum. b) The number of NMP molecules confined between the two graphene monolayers [66]. 90
Figure 9: Interaction potentials, represented by the potential of mean force per unit area, between two graphene sheets in a) NMP, DMF and Water, and b) in an aqueous surfactant solution using Sodium Cholate (SC). Data points are MD simulation data from [66] and [71].....91
Figure 10: Schematics of the conversion of bulk graphite into graphene oxide with corresponding micrographic images or sample appearances at each phase. The three steps indicate the formation of the two intermediate products (graphite intercalated compound, GIC, and pristine graphite oxide (PGO)) and the final GO product. The solid black lines represent graphene layers; dotted black lines represent single layers of GO; wide blue lines represent H_2SO_4/HSO_4- intercalant; wide purple lines represent a layer of the mixture of H_2SO_4/HSO_4- intercalant with the reduced form of oxidizing agent. Reproduced with permission from ref.[175]. Copyright 2014 American Chemical Society.....92
Figure 11: Schematic overview of cathodic and anodic exfoliation mechanisms. A positive or negative charge is created at a graphite working electrode, attracting oppositely charged intercalating ions. Reproduced with permission from ref. [89]. Copyright 2015 Elsevier B.V. 93
Figure 12: Schematic illustration of solvothermal-assisted exfoliation and dispersion of graphene sheets in acetonitrile: a) pristine expandable graphite. b) expanded graphite. c) schematic showing the insertion of acetinitrile molecules into the interlayers of expanded graphite. d) exfoliated graphene sheets dispersed in acetonitrile. e) optical images of four samples obtained under the different conditions described in Table 2. Reproduced with permission from ref. [26]. Copyright 2009 Tsinghua University Press and Springer Berlin Heidelberg. 94
Figure 13: Overview of the microwave-assisted liquid-phase exfoliation of graphite in ionic liquids with a schematic of the 'reaction' set-up. Typically, a vial containing a graphite suspension in ionic

liquid was placed in a glass reaction vessel. This vessel was then placed in a microwave reactor operating at 2.45 GHz and irradiated using a single-mode microwave setting at 30 W for 30 min. The microwave-irradiated mixture of graphite in ionic liquid was diluted with dimethylsulfoxide (DMSO), and the entire mixture was transferred to a PTFE thimble filter. The solid residue in the thimble filter was rinsed successively with DMSO (reduced pressure; ~30 mmHg), 2,2,2-trifluoroethanol and dichloromethane by using a Soxhlet extraction system, and subsequently dried under reduced pressure to create a black powder (bottom right) that contained 95% single-layer graphene (93% yield). Reproduced with permission from ref. [24]. Copyright 2015 Nature Publishing Group.....95

Figure 14: a) Schematic of the exfoliation of graphite using a supercritical fluid (i.e. CO_2). In this instance, graphene was simultaneously modified with pyrene-derivatives. b) Schematic of an experimental device to exfoliate graphite using a supercritical fluid. Reproduced with permission from ref. [43,84]. Copyright 2013 American Chemical Society, Copyright 2016 Elsevier. 96

Figure 15: a) Schematic of the vortex fluidic device used to exfoliate graphite and boron nitride (10 mm diameter tube, 16 cm long, inclined at 45°, operating at 7000 and 8000 rpm for graphite and boron nitride, respectively). b) Photographs of the resulting colloidal suspensions of graphene (top) in NMP. Illustrations of c) the microfluidic flow velocity indicted by red arrows for a section of the rotating tube; d) the exfoliation process; and e) slippage on the inner surface of the tube. Reproduced with permission from ref. [100]. Copyright 2012 The Royal Society of Chemistry. 97

Figure 16: Schematic of the shear-exfoliation of graphite into few-layer graphene by a Taylor Vortex flow. Photographs shows a Taylor–Couette flow reactor and the graphene dispersions produced by shear exfoliation. The volume in the reactor for mixing was 200 mL, and the gap between the two concentric cylinders was 2.5 mm. Reproduced with permission from ref. [102]. Copyright 2016 The Royal Society of Chemistry. 98

Figure 17: a) Schematic of the spinning disc processor used for exfoliation of graphite (20 cm diameter stainless steel disc operating at 2500 rpm). b) Proposed mechanism of exfoliation and

scrolling of graphite and boron nitride flakes using the set-up. c) TEM image of partial carbon nanoscroll. Reproduced with permission from ref. [103]. Copyright 2012 The Royal Society of Chemistry. 99

Figure 18: a) 3D sectional drawing of a high-shear mixer for the production of graphene. b) Main energy dissipation regions of the high-shear mixer (sectional view). c) Schematic of preparing graphene nanosheets by shear force, collision and jet cavitation. Reproduced with permission from ref. [41]. Copyright 2014 The Royal Society of Chemistry. 100

Figure 19: Overview of the outputs using a high shear mixing process for exfoliation. a) Phase diagram of rotor speed, N, versus diameter, D, for dispersions showing good exfoliation according to TEM. The region above the black line represents fully developed turbulence, that is, $Re_{Mixer} > 10^4$, whereas the region above the red line represents $\dot{\gamma}$ min $>10^4$ s^{-1}. b) Concentration of graphene produced in the Silverson shear mixer as a function of shear rate for rotors with diameters of 32, 16 and 12 mm (mixing time 1 min). All three data sets are consistent with the same minimum shear rate. Reproduced with permission from ref. [40]. Copyright 2014 Nature Publishing Group. 101

Figure 20: An illustration of the mechanical mechanism for exfoliation via sonication. Reproduced with permission from ref. [84]. Copyright 2015 The Royal Society of Chemistry. 102

Figure 21: Concentration of graphene after centrifugation as a function of sonication time. On the left axis is the measured absorbance per cell length, A/l, while the right axis corresponds to the concentration calculated using an absorption coefficient of 3620 mL mg^{-1} m^{-1}. The upper axis shows the total energy outputted by the bath calculated using the measured power output of 23 W. Reproduced with permission from ref. [20]. Copyright 2010 John Wiley & Sons, Inc. 103

Figure 22: a) Schematic of the cavitation generator. b) Illustration of the mechanisms during the production of graphene flakes by jet cavitation. Reproduced with permission from ref. [115] . Copyright 2014 Springer. 104

Figure 23: a) Schematic of a typical setup for the electrochemical exfoliation of graphite. b) A novel setup for continuous electrochemical exfoliation process. Reproduced with permission from ref. [89]

and [118]. Copyright 2011 American Chemical Society, Copyright 2014 American Chemical Society. 105

Figure 24: a) Schematic representation of the electrochemical micro-reactor combining electrochemical exfoliation and shear-driven exfoliation. The graphite crystal is both the wall and the working electrode of the reactor and simultaneously experiences a high wall shear rate and an applied electric potential. Here H, Q, and $\dot{\gamma}$ are the height between two electrodes, electrolyte flow, and shear rate, respectively [54]; b) Effect of potential and shear rate on the size of graphene flakes produced in the flow reactor. A mean size distribution of zero, specifically in the case for only potential and shear rate of 6925 s^{-1}, indicates that exfoliation was unnoticed over the samples that were measured. The green and blue colors in the figure indicate shear and potential dominated regions, respectively. Statistical flake size analysis for the graphene was performed using more than 80 sheets from AFM measurements. Error bars in these figures are from three samples at a given condition, showing the maximum and minimum values. Reproduced with permission from ref. [54]. Copyright 2016 American Chemical Society. 106

Figure 25: A summary of the top-down production considerations in the scale-up of graphene 107

1. Introduction

Nanomaterials have emerged as a critical sector that is likely to push the frontiers of technology. The remarkable properties which carbon nanomaterials boast, such as high electrical and thermal conductivities and tensile strength, offer a strong platform to exceed the current boundaries imposed in several fields of science and engineering. Within these fields, the application of fundamental chemical engineering concepts is crucial to understanding low-dimensional nanomaterials [1]. Two-dimensional (2D) materials are one type of nanomaterial which is receiving considerable attention, the most featured one being undoubtedly graphene, a semi-metal that consists of a flat monolayer of carbon atoms [2]. This carbon monolayer is densely packed into a 2D honeycomb lattice and has fully conjugated sp^2 hybridised planar structure with carbon-carbon bond length of 0.142 nm. Due to its two-dimensional nature, graphene has a unique range of properties and is part of a family of carbon-based materials with other dimensionalities e.g. 3D graphite, 1D nanotubes, and 0D fullerenes.

Scientific research on graphene over the past decade has demonstrated a remarkable range of properties. The electron mobility at room temperature can reach > 250,000 $cm^2\ V^{-1}\ s^{-1}$ [3]. It can deliver a maximum current density that is more than several million times higher than that of copper. Thermal conductivity and mechanical properties have also shown astonishing results. It has a thermal conductivity of approximately 3000 $W\ m^{-1}\ K^{-1}$ [4], a Young's modulus of 0.5–1.0 TPa and a high intrinsic strength of approximately 130 GPa [5]. Moreover, its transmittance reaches about 97.7% [6] and it has extremely high resistance to gas permeation [7]. Given the extraordinary breadth of high performing properties from this single material, and the recent emergence of other 2D materials such as boron nitride nanosheets (BNNS), transition metal dichalcogenide monolayers (TMDs) and transition metal oxides (TMOs) also showing exceptional characteristics [8,9], this area of nanomaterials can play a major role in the future development of applications that will have tremendous economic

and societal impact; these include optoelectronics, sensors, tissue engineering, drug delivery, energy conversion, and storage.

Despite the extensive list of potential end-uses, the implementation of graphene and other 2D materials into practical applications is currently limited. There is widespread consensus within the scientific community that this is primarily attributed to the limitations of large-scale production strategies. A review by Ferrari *et al.* [10] on the scientific and technological developments of graphene concluded that widespread practical implementation will be enabled once each production route is at a sufficiently mature stage.

In general, there are two ways to categorise the production of graphene: 'bottom-up', and 'top-down'. Bottom-up techniques involve the utilisation of chemical reactions to produce 2D graphene from hydrocarbon precursors, and include processes such as chemical vapour deposition, arc discharge, and epitaxial growth. The top-down approach uses graphite as a precursor, which is a crystalline material that is essentially constructed from multiple graphene sheets with an interplanar spacing of 0.335 nm. By exceeding the critical exfoliation energy of approximately 2 eV nm^{-2} [11], van der Waals forces between the graphene sheets are overcome, thereby deconstructing graphite into sheets of graphene. These sheets must then be held in an environment that minimises the potential for re-stacking, commonly achieved using appropriate solvents or aqueous surfactant solutions. Top-down approaches, that can produce graphene in this liquid carrier fluid, also indirectly benefit certain end-use applications such as the deposition of graphene films for fabrication of photonic devices with both transparent and conducting properties[12].

An obvious route towards reducing the cost of mass-production is through the development of methods that can deliver high yield and production rates. The material properties are also sensitive to the approach [13], which makes the production challenges complex and multifaceted. Many of the

contemporary bottom-up and top-down production approaches have evolved over the last ten years. The aim of the current review, therefore, is to provide an overview of the present status of large-scale graphene production. Particular emphasis is placed on the top-down route, highlighting the mechanisms, dispersion, advantages and limitations of the existing techniques. Non-oxidizing liquid-phase exfoliation has shown potential for scaling-up the production of high quality graphene within this domain.

2. Publications and patents

The emerging area of graphene production is receiving extensive attention, and a continuation of these research efforts can only benefit the future implementation of efficient production technologies. Within the broader context of graphene research activities, however, investigations on production are a fraction of the total. This is illustrated in Figure 1 by the number of publications and patents on these topics since 2000. As of 2016, publications under the topic of graphene production account for less than 5% of the total. Although it is a relatively low contribution (It is worth noting that the search terms "graphene" and "production" do not capture all studies on graphene production), the outlook appears promising when the yearly growth is examined from this historical information.

FIG 1

The trends in research activities over the 2000-2016 duration are presented in Figure 2. For both graphene and graphene production, there are two trends which describe a before and after state when research efforts increased considerably. For graphene research, there is no doubt that the breakthrough by Novoselov *et al*. [2] changed the broader graphene research path. The scientific output increased two orders of magnitude over a decade from this point in time. Figure 2 also shows that an equivalent point in time, where attention on the production of graphene began to increase, arrived about two years later. Since 2007, the rate of scientific output in this field has grown each year to a cubic power law ~ t^3. Given that this output is growing at a rate that is slightly above the overall graphene research

output, the outlook for continued development and refinement of production approaches is encouraging.

FIG 2

A breakdown of the generation of intellectual property (IP) through patents goes some way towards understanding the importance of graphene production to the industrial sector. Figure 1 b) presents a non-comprehensive gathering of the number of patent applications, providing a sample view on the landscape. In contrast to the scientific output, production aspects are a much higher fraction at almost 15% of the general graphene IP area in 2015. The difference between scientific output and generation of IP is not surprising, given that mass-production is a topic directly linked with industrial practices. Economic factors may also have an influence. A recent forecast for 2017 predicts that material supply will account for $75M of a >$250M graphene/2D material global market, which includes end-use applications [14]. As the graphene technology space develops, it is expected that a re-distribution in IP will occur from production/synthesis towards end-use applications of graphene and graphene-related materials [10].

3. Graphene-based materials

The type of material produced by bottom-up and top-down approaches varies depending on the production method. In Figure 3, schematic representations of these different types of materials are provided together with corresponding transmission electron microscopy (TEM) images of their respective morphologies. Bottom-up approaches typically produce monolayer graphene and multi-layer graphene (MLG, $2 < N_l < 10$), with highly-controlled layer numbers (N_l). Top-down approaches utilise graphite ($N_l > 10$) and exfoliate this precursor into monolayer and multilayer graphene with a broad distribution in layer number. Top-down approaches which implement chemical and electrochemical exfoliation mechanisms produce graphene oxide (GO), a form of graphene that includes a high oxygen content resultant from the exfoliation process. Further post-processing of GO, to reduce the oxidation state and increase electrical and thermal conductivities, produces reduced

graphene oxide (rGO). In these forms, GO and rGO can be useful for certain applications such as energy storage and composite materials [10]. There is an intrinsic relationship between the different production methods and the type of graphene-based material that is produced, as illustrated in Figure 4. Although the focus of this review is on graphene production methods, the reduction approaches discussed below have been included for completeness.

FIG 3

4. Existing production routes

The 'bottom-up' and 'top-down' approaches are illustrated in Figure 4. Graphene of high quality can be produced through bottom-up approaches, which is suited for use in electronic devices. These techniques, however, have generally suffered from very low production rates. In contrast, top-down processes, which most commonly use liquid-phase exfoliation, produce graphene at much higher production rates but often result in noticeably lower quality. The re-stacking of the sheets produced is commonly restricted using suitable solvents or aqueous surfactant solutions (see Section 5.2). The resulting graphene has been typically reserved for composites, conductive inks, coatings and flexible electronics applications.

FIG 4

Providing direct comparisons between the two production routes is challenging. Each route holds particular advantages and disadvantages in terms of use of feed materials and energy, pre- and post-processing requirements, graphene product specifications, technology and process complexity, environmental sustainability, and many other important aspects. Similarly, the properties required for the end-use application may determine the choice of production route. There are many applications where graphene of the highest quality and aspect ratio (lateral size to thickness ratio) is unnecessary. Considering the breadth of applications mentioned previously, it is probable that top-down approaches will provide the primary source of mass-produced graphene in the near future. The demand for graphene produced via top-down methods will, therefore, be influenced by the broad

interest in graphene-based technological developments from various industries. If there is going to be a stable and growing demand for a lower quality graphene produced via top-down methods, it should encourage graphene producers to develop novel top-down processes, with the aim of improving process intensification and material quality.

Furthermore, top-down approaches principally offer more financially feasible production (continuous or batch) of graphene at a large-scale relative to bottom-up methods. Many of the top-down methods developed can be easily integrated with other widely used processes to either modify graphene for distinct applications, or to use it directly in processes such as chemical functionalisation, surface modification, and film deposition [15]. Despite these process integration benefits, the most widely researched methods such as liquid-phase and electrochemical exfoliation, require substantial improvements in process efficiency, sustainability, and monolayer production yield, for feasible scale-up.

When choosing to further advance a particular graphene production route, it is preferential to evaluate key characteristics such as the production yield and throughput. An example of such evaluation is presented in Figure 5, which summarises the data reported in a selection of studies on graphene production via top-down and bottom-up methods [16-29]. This type of data set highlights key production outputs, and provides a clear comparison between the methods based on their important features. For instance, the arc discharge method can potentially produce graphene at relatively high rates, but it suffers from having low production yield. If one can consider advancing or optimising process conditions, then this could probably lead to an improvement of graphene production yield. Similarly, methods that produce graphene at a high yield but at low rate e.g. microwave and ball milling, can be evaluated to understand the relationship between both variables and increase throughput. Although those methods that suffer from both low production rate and yield present risks from a technological viability perspective, these may also give opportunities to explore the production of targeted products

e.g. perforated graphene via pressure driven methods, or use of sonication for post-production and storage. As noted previously, such analysis must encompass other key measures such as graphene defects, selectivity, target properties, input and operation costs.

FIG 5

5. Liquid-phase exfoliation

The top-down route to production of graphene encompasses a wide range of methods that use a graphite precursor as a starting material. Liquid-phase exfoliation is the most common area of research in this field, where the graphite precursor is exfoliated directly within a liquid. Three main approaches that have emerged over the past decade are discussed. These have been grouped into Mechanical, Chemical, and Electrochemical exfoliation. This section explores the key factors that impact the scale-up of production including the precursor, the dispersion medium, the exfoliation mechanisms and the current techniques.

5.1 Precursor

Graphite is the main raw material (apart from other chemical precursors and dispersants, see Section 5.2) used in top-down methods of graphene production. Graphite itself is produced either naturally or synthetically, and consists of polycrystalline particles or granules which are composed of multiple single crystals. In natural graphite, these crystals are orientated in a preferred direction, whereas the orientation in synthetic graphite is more random. Graphite consists of multiple 2D graphene layers, held in parallel to each other by van der Waals forces, forming a 3D crystal. These layers are organised to create a stable structure with a particular stacking sequence. The most common sequence is hexagonal (ABAB…), whereas rhombohedral (ABCABC…) is rather rare [30].

Both natural and synthetic graphite materials have many different varieties e.g. ‘amorphous’ graphite, flake graphite, vein graphite, high purity flake graphite, expanded graphite, highly oriented pyrolytic graphite (HOPG), Kish graphite, etc. [31]. Different types of graphite of particular grain sizes and

purities have been used by other researchers, and this information is displayed in Table 1. All of these types of graphite variations have differences, either small or large, in their physical and chemical properties. These differences include particle size distribution, morphology, and purity (see Figure 6 for a more detailed breakdown). The properties play a critical role, not just in the control of the exfoliation process and the quality of the graphene output, but the applicability of the graphene in downstream industrial processes. It is necessary to have a thorough understanding of the raw material characteristics, since the fundamental exfoliation mechanisms are occurring at the nanoscale.

Five different types of graphite materials (HOPG, natural graphite flake, Kish graphite, flake graphite powder, artificial graphite) were used by Wu *et al*. to produce graphene using a chemical exfoliation method. These materials have different lateral sizes, thicknesses, morphologies and purities. It was found that the selectivity of the number of graphene layers is strongly correlated with the lateral size and crystallinity of the precursor graphite. As the lateral size and crystallinity of precursor graphite decreases, the thickness of the produced graphene also decreases [32].

Similar observations were made by Knirsch *et al*. in a study on the chemical reactivity of three different graphite sources. This included graphite flakes, graphite powder and spherical graphite. All three precursors have different morphologies, density of defects and bulk densities. Their analysis showed that powder graphite yields the highest degree of functionalization – (I_D/I_G) average = 3.1. They also confirmed that larger graphite flakes undergo only partial exfoliation, due to higher intrinsic lattice energy [33]. The significance of natural graphite particle size was also carefully studied by Arao *et al*. It was shown that the production of few layer graphene is much more efficient when small graphite particles are used relative to larger graphite particles. Their findings also add to the fact that the energy required for exfoliation increases with increasing graphite particle size [34].

Kozhemyakina *et al*. used 22 different graphite grades to study their dispersibility in various solvents. This study allowed them to clearly identify that the smaller graphite particles (relative to larger ones) can be more readily dispersed in a solvent and form a more stable dispersion. This can be even further enhanced if graphite of small bulk density and pH close to neutral in water is used [35].

Considering other graphite properties, the presence of impurities such as iron in flake and Kish graphite will result in paramagnetic properties, which can be either beneficial or undesirable as a precursor material for particular applications. For instance, graphene with iron could be used in the manufacture of composites and thin film conductors, but it would be undesirable to use it in spintronic or magnetic applications [36].

Graphite can also be pre-treated to encourage exfoliation, and potentially increase the production yield of high quality graphene with high aspect ratio. An intercalation process could be employed to produce expanded flake graphite. This pre-treated precursor could then be used in an exfoliation process to produce graphene with beneficial properties, such as high electrical conductivity [37]. This pre-treatment, however, should be thoroughly controlled and assessed to mitigate any unwanted changes in important graphene properties. This topic requires a comprehensive research effort, to understand the defects introduced, how these arise and how these could be potentially healed [38]. If graphene of very high quality and purity is required, such as in the electronics industry, HOPG is one of the desirable starting materials. The limited supply of HOPG, however, makes it currently financially unviable for large-scale production.

It is crucial, therefore, that graphene producers at least consider the type and grade of graphite to be used, including grain size, density and purity. Control over the precursor characteristics translates into a finer control over the exfoliated product. This can also benefit downstream industrial use of graphene produced using top-down methods. Employing collaborative research efforts, between

graphite producers in industry and academic institutions investigating top-down production methods, could be a key driver in the advancement of optimal, economically viable precursors.

FIG 6

Table 1: Summary of different graphite precursor used in the literature to produce graphene.

Type	Grade	Purity	Size	Ref.
Graphite flakes, natural	n/a	n/a	+100 mesh (≥75% min)	[39]
Graphite flakes, natural	n/a	n/a	+100 mesh (≥75% min)	[40]
Graphite flakes, natural	n/a	96 %	>32 mesh	[40]
Graphite flakes, natural	n/a	n/a	+100 mesh (≥75% min)	[18]
Graphite flakes, natural	n/a	99.80 %	325 mesh	[41]
Surface enhanced flake graphite, natural	Grade 3725	n/a	< 3 µm	[37]
Graphite flakes, natural	HP230U	99.60 %	20 µm	[42]
Expandable graphite, natural	n/a	99 %	average diameter of 300 µm	[26]
Expandable graphite, natural	Grade 3772	99.35 %	20 x 50 mesh	[37]
Expanded graphite, natural	n/a	99.50 %	10–30 µm	[43]
Graphite powder, natural	n/a	n/a	0.5 mm mesh	[44]
Graphite powder, natural	n/a	n/a	<0.1 mm	[45]
Flake graphite powder, natural	n/a	> 99.9 %	25 µm	[46]
Powdered graphite, natural	n/a	≥ 99.99 %	~70 µm	[47]
Graphite powder, natural	n/a	≥ 99.99 %	100 mesh	[48]
Crystal graphite powder, natural	n/a	≥ 98.0 %	≤ 300 mesh	[49]
High purity graphite rods, natural	n/a	≥ 99.99 %	diameter 6 mm	[50]
Primary artificial, synthetic	Grade TC307	≥ 99.9 %	< 1µm	[37]
Graphite powder, synthetic	n/a	≥ 99.99 %	1–10 mm	[51]
Graphite powder, synthetic	n/a	n/a	< 20 mm	[52]
Graphite powder, synthetic	SP-1	≥ 99.99 %	100–200 mm	[51]
HOPG	SPI-2 grade	≤ 10 ppm ash	10x10x1 mm	[53]
HOPG	SP-1	n/a	10 mm × 10 mm × 0.2 mm	[54]
HOPG	n/a	n/a	1 x 1 cm^2	[55]
HOPG	n/a	n/a	n/a	[56]

5.2 Graphene dispersion

In addition to the precursor material, another key component of the exfoliation process is the selection of an appropriate liquid medium. Graphene concentration benefits when suitable liquids are used to separate nanosheets from the graphite precursor, and inhibit the thermodynamically favourable aggregated state for long periods of time. Solvents and aqueous surfactant solutions are the predominant routes for the metastable dispersion of pristine graphene in non-oxidative liquid phase exfoliation techniques. In addition, an approach known as "Reductive Dissolution" has been shown to produce thermodynamically stable liquid formulations of nanocarbons. This chemical method spontaneously deconstructs a graphite intercalated compound into its constitutive graphene layers. A brief summary of this dispersion approach has also been included. In all cases, there has been an increased effort over the past decade to characterise the dispersive performance of liquids, and obtain fundamental information on molecular-scale interactions.

5.2.1 Solvents

Solvent-based exfoliation of graphene has become the most common route in liquid-phase exfoliation production methods. This approach to exfoliation of graphene has its origins from earlier work on the exfoliation and dispersion of carbon nanotubes [57-61]. Challenges in aggregation and bundling of single-walled carbon nanotube (SWCNT) powders were addressed through dispersion in suitable solvents. These solvents balance the attractive potentials with repulsive potentials, preventing aggregation and stabilizing the mixture, once the bundles of nanotubes are exfoliated. This aggregation is a fundamental result of van der Waals interactions between carbon atoms in adjacent nanotubes [58].

The physics of this mutual attraction is similar for graphene nanosheets. Additionally, the similarity between recently proposed solvent parameters [62] and surface energies [63] suggested that solvents used

in SWCNT studies could also be used to exfoliate graphite into graphene. This is the reason, therefore, that many of the "good" solvents originally used in SWCNT dispersion are also common in the more recent research on liquid-phase exfoliation of graphene. Towards the end of the last decade, a comprehensive experimental campaign was undertaken to analyse the effectiveness of numerous solvents to exfoliate and disperse graphene [18,62]. Hernandez *et al*. [62] presented graphene concentration data for 40 different solvents. Cyclopentanone (CPO) provided the highest concentration, and N-Methyl-Pyrrolidone (NMP) was also a high performing solvent. The latter has become one of the most popular solvents in liquid-phase exfoliation studies to date. Water was a poor solvent for graphene exfoliation and dispersion, positioned 35 out of 40, and providing concentrations 1/8 of that achieved with CPO. This highlights one of the primary challenges in scaling-up solvent-based liquid-phase exfoliation. Many of the good solvents, such as NMP, have a high boiling point and are toxic.

In an effort to correlate the experimental findings, and provide a physical interpretation behind the solvent ordering, the authors considered surface energy as a parameter [18] along with Hildebrand and Hansen solubility parameters [62]. The overarching idea, linked to similar work on SWCNTs [64], is that suitable solvents can be selected through minimization of the enthalpy of mixing. The initial work proposed that matching solvent and graphite surface energy would minimize the energetic cost of exfoliation. The recommendation was the use of solvents with surface tension close to 40 mJ/m^2. In a follow-on study, Hernandez *et al*. [62] suggested that although surface tension is a useful parameter to assess the overall interaction, the intermolecular interactions could be divided into at least three types based on the Hildebrand and Hansen solubility parameters. The cost of mixing solute-solvent was related to the Flory-Huggins interaction parameter, which scales as $\chi \backsim R^2$. Here, R represents the Hansen solubility sphere between solute (1) and solvent (2), and $R^2 = 4(\delta D_1 - \delta D_2)^2 + (\delta P_1 - \delta P_2)^2 + (\delta H_1 - \delta H_2)^2$. The dispersive, polar and hydrogen-bonding components are defined by $\delta D, \delta P$ and δH respectively [65]. The cost of mixing is, therefore, reduced when small values of R are achieved. This is the commonly known "like dissolves like" concept.

Hansen parameters are regularly used in molecular solubility analyses, and their applicability to treat nanomaterials (with well-defined surfaces) as a classical solute remains questionable. To illustrate this, Figure 7 a) presents the parameters for the solvents from the previous graphene exfoliation studies in three-dimensional Hansen space. The radius of each data point is scaled with respect to graphene concentration after centrifugation. The Graphene Sphere R_{NMP} represents the relative energy distance for graphene and NMP as a solvent. The solubility parameters for graphene were estimated as $\langle \delta D \rangle \approx 18, \langle \delta P \rangle \approx 9.3, \langle \delta H \rangle \approx 7.7$ (units: $MPa^{1/2}$) [62]. This example was chosen given the widespread use of NMP in the liquid-phase exfoliation of graphene.

Taking a rigorous interpretation of the Hansen solubility sphere, if NMP is a good solvent than any other solvent within this sphere should also be equally good (or better) for exfoliation and dispersion of graphene. In this case, only six solvents of the top ten are within this sphere (Figure 7 b), with the best solvent CPO outside. There are also poorer solvents, such as Pyridine, within this bounded space. Similarly, there is a scatter of good and poor solvents that have a surface tension close to 40 mJ/m^2. Figure 7 b) implies that if a particular solvent is to be classified as good, then it will most likely have a surface tension within the 35 - 45 mJ/m^2 range. Put another way, it is not guaranteed to be a good solvent if it has the recommended surface tension of 40 mJ/m^2. The same probabilistic interpretation appears to also apply in the application of Hansen solubility parameters to graphene-solvent dispersions. This suggests that, although these empirical reduction methods hold merit in guiding the search for suitable solvents to exfoliate and disperse, fundamental insights at the material-solvent interface are required.

FIG 7

Molecular-scale simulations of monolayer graphene sheets in solvents provides the opportunity to study this material-solvent interface in detail. Shih *et al*. [66] produced a thermodynamic description of the stability of graphene in five polar solvents (NMP, DMSO, DMF, GBL, and water) using

Molecular Dynamics (MD). Two parallel monolayer sheets were simulated in a domain comprising the solvent of interest. The distance between both sheets, *d*, was varied to understand the interaction. This interaction, when using NMP as a solvent, is shown in Figure 8. The solvent has two beneficial characteristics which both aid exfoliation concentration and reduce aggregation. Firstly, the van der Waals energy well is shallower than that for two graphene sheets in vacuum. Secondly, a high energy barrier exists, which must be overcome if graphene sheets are to aggregate. Comparing the potential of mean force (PMF) with number of NMP molecules as distance is decreased, the rapid change in peak energy at $d = 0.66$nm corresponds to the desorption of a single layer of NMP molecules that are positioned between the graphene sheets. This occurs when the total potential energy of the confined solvent molecules exceeds the bulk solvent-solvent potential energy. The van der Waals interaction between the graphene sheets, therefore, dominates in the absence of NMP molecules at $d < 0.66$nm.

As a way to illustrate why certain solvents are good/poor, based on the findings of Shih *et al.* [66], Figure 9 a) presents the PMF per unit area for NMP (good), DMF (good) and water (poor) examples. Both NMP and DMF have similar magnitudes for the van der Waals energy well and the high energy barrier, with NMP performing slightly better. Graphene can remain dispersed, even though the ultimate thermodynamic equilibrium state is in the aggregated form (i.e. graphite). The 2D sheets can be held in a kinetic or metastable state for a long period of time if this energy barrier is sufficiently large [67]. The larger the energy barrier, the slower the kinetics, which explains why NMP has been shown experimentally to be one of the most suitable solvents for long term dispersion. In contrast, the depth of the energy well for water is almost double that of the good solvents, and the energy barrier is extremely low.

Shih *et al.* [66] also produced a fit of the numerical data, to capture the effect of the confined single layer of solvent molecules. The fit is based on the classical Lennard-Jones potential, with additional terms to model the energy barrier and secondary energy well contributions. This is shown in Figure

9 a), and provides a useful insight for the molecular design of solvents that can enhance exfoliation and dispersion. The PMF results were combined with theory of slow colloid coagulation, to compare time-dependent aggregation observations with experiment. In NMP, the fraction of monolayer graphene can reduce from 27% to just 9% after 10 days as sheets aggregate. This highlights the considerable challenge in enabling long-term storage, as NMP is currently one of the most efficient solvents for liquid-phase exfoliation. Overall, the predictions provided a fundamental insight into the molecular stabilization mechanisms and a practical tool for the determination of time-dependent aggregation in solvents.

FIG 8

FIG 9

5.2.2 Surfactants

Surfactants can be used to lower the surface tension of water, making this environmentally benign solvent suitable for the dispersion of graphene. Surfactant-based exfoliation and dispersion addresses some of the disadvantages associated with the use of solvents. Aqueous dispersions using surfactants have a low boiling point, compared to the widely used solvents, and also have environmental benefits. One of the limitations, however, is the adverse effect residual surfactant can have on the electronic properties of graphene. This can result in a need to remove the surfactant in a post-processing step, such as immersion in nitric acid for a period of time and rinsing with deionized water [68]. A positive impact is that the electronic structures can be fully recovered. The negative is that a further processing step is required with additional chemicals, leading to increased cost in scale-up. Unsurprisingly, the choice of surfactants in liquid-phase exfoliation of graphene also originated from the earlier work on carbon nanotubes [60,69,70]. The Vigolo *et al*. study[69] was one of the earlier works that assessed the influence of the surfactant sodium dodecyl sulphate on the dispersion performance of carbon nanotubes in water solution. Phase diagrams were used to show the influence of both surfactant and carbon nanotube concentrations on the level of homogeneity in the dispersion. Lotya *et al*. [44] used sodium dodecylbenzene sulfonate (SDBS) to demonstrate exfoliation and dispersion of graphene

using sonication. The relatively stable dispersions were then used to produce films with vacuum filtration and spray coating.

Surfactants can promote graphene dispersion through the formation of an electric double layer, or alternatively, a steric stabilization effect [67]. An electric double layer is repulsive, preventing the attractive van der Waals potential from aggregating the individual monolayer or few-layer graphene sheets. The repulsive electrostatic potential for two monolayer sheets separated by distance, *d*, is presented in Figure 9 b) using DLVO theory [67,71].

A steric repulsion can be formed when the hydrophobic tail of a surfactant molecule adsorbs to a graphene sheet. The hydrophilic component extends into the water, and interacts with other hydrophilic parts when surfactant coated graphene sheets come into close proximity [27]. This compressive interaction has an unfavourable entropy, resulting in a steric repulsion potential [67].

The quantity of monolayers produced with surfactants was found to be lower than that achieved using solvent based exfoliation [72]. Lotya *et al*. [73] produced a maximum of 0.3 mg/mL of graphene for a prolonged 430 hours of sonication time. The optimal concentration of sodium cholate (SC) in water was found to be 0.1 mg/mL. With the same surfactant concentration, Smith *et al*. [27] tested 12 ionic and non-ionic surfactants for direct comparisons. The comparison between both types of surfactants also provided an insight into both the electric double layer and steric stabilization mechanisms. The length and thickness of the exfoliated sheets was similar for all, however, concentration ranged between 0.011 and 0.026 mg/mL. Part of this variation may have also been related to the application of non-optimal surfactant concentrations. In 10 of the 12 cases studied, the concentration was well below the critical micelle concentration [67]. One advantage of this, however, is that it results in less surfactant removal during the post-processing steps. Overall, there appeared to be minimal differences between the maximum concentrations achieved using ionic and non-ionic surfactants.

Guardia *et al*. [45] however, measured substantial improvements using non-ionic over ionic surfactants. Concentrations of graphene were also produced at much higher levels up to approximately 1 mg/mL. Given the impact of surfactants on production output and material electronic properties, there has been a desire to optimise surfactant concentrations[74]. Sun *et al*.[75] maximised graphene concentrations up to 7.1 mg/mL using sodium taurodeoxycholate and tip sonication (90% graphene < 5 layers).

Even higher graphene concentrations, up to 50 mg/mL, have been obtained using a flavin mononucleotide (a derivative of vitamin B_2) stabilizer in water[76]. Biomolecule-assisted exfoliation is another relevant field that has recently emerged[77]. Dispersion of graphene has been achieved with biomolecules including proteins and peptides, RNA, DNA, plant extracts and bile salts. The principle dispersion mechanisms are similar as that discussed here for surfactants. Further details on this area of research and end-use applications have been reviewed recently[77].

Simulations of monolayer sheets in aqueous surfactant solutions have also led to an improved understanding of surfactant dispersed graphene at the molecular scale [71]. Figure 9 b) describes the interaction potentials with sheet separation distance for two graphene monolayer sheets. These potential mean force predictions are the equivalent to that shown in Figure 9 a) for polar solvents. A deviation between DLVO theory and the molecular dynamics predictions occurs in the near-field region, where d = 1.6 nm. Beyond d = 1.6 nm, there is reasonable agreement, as the long-range electrostatic repulsion is the interaction potential which dominates. This electrostatic contribution is captured by DLVO theory [67].

In the near-field, an energy barrier is produced by steric repulsion, as the surface adsorbed cholate ions come into contact with each other. A metastable well, at d = 1.05 nm, features a single layer of cholate ions and a sodium-ion wall confined between both sheets [71]. Most notably, this study highlights that the electrostatic interaction is not the dominant repulsive force as assumed previously

for ionic surfactants [27]. This comes primarily from the steric repulsion in the last layer of sodium cholate (SC) confined between the graphene sheets. The inset model, fitting the data in Figure 9 b), is similar to that proposed in the original study on solvents [66]. This potential mean force model was ultimately used to predict the time-dependent concentration of graphene using colloid aggregation theory. This forms a useful engineering tool for estimating monolayer lifetimes in aqueous surfactant dispersions. Graphene concentrations in SC have been found to reduce by almost 70% in 10 days [71]. Predicted monolayer number fractions become depleted, as more few-layer sheets (N > 3) are formed through aggregation. As with solvent dispersions, one of the main process engineering challenges will be to maintain an as-exfoliated layer distribution throughout long-term storage.

5.2.3 Reductive dissolution

Once the liquid phase exfoliation mechanism is stopped, both traditional solvent and surfactant-based dispersions of graphene ultimately return to an aggregated state over time due the conditions being thermodynamically unstable. An alternative chemical processing approach is reductive dissolution, which wholly deconstructs graphite particles into their constitutive graphene flakes and maintains dispersion in a liquid [78]. This feature yields a stable, spontaneously soluble graphene product, which the previous dispersion mechanisms have yet to demonstrate.

The dissolution process uses a graphite intercalation compound (GIC), such as potassium graphite KC_8, as the precursor material. Electrostatic interactions occur between graphene layers, and these two-dimensional negatively charged flakes are dissolved spontaneously in a polar solvent such as NMP. This occurs as the favourable entropic term ($T\Delta s$) in the free energy of mixing relationship ($\Delta G = \Delta h - T\Delta s$) dominates the unfavourable enthalpic contribution (Δh), similar to that described for the dissolution of nanotubes [78,79]. Due to the charged nature of the material, leaders in this field have labelled the product as graphenide [80] to distinguish it from neutral graphene. This follows the terminology introduced for dissolved carbon nanotubes (nanotubides [79]) and fullerenes (fullerides [81]).

The spontaneous dissolution process has a number of advantages as a production route. Both quality and quantity are high relative to the methods of mechanical exfoliation in liquids. Lateral flake sizes are large (50 μm shown in Ref. [80]), as the dissolution process inherently avoids the fragmentation mechanisms that are common in other liquid phase exfoliation methods such as sonication. The approach has been shown to work with other low boiling point solvents[82], thus addressing the process and environmental challenges associated with scaling up production with the commonly used solvents discussed in Section 5.2.1. A disadvantage, however, is that the solutions must be processed in an inert atmosphere. The effects of the intercalation process, have been shown to be relatively minor, and the work function can be similar in magnitude to that of undoped graphene.

Recently, negatively charged graphene has been dispersed in water without surfactant using the product derived from this reductive dissolution method[83]. In this breakthrough, graphenide and tetrahydrofuran were mixed with degassed water. The organic solvent was evaporated off to leave graphenide dispersed in water at a concentration of 0.16 g/L. For further information on the reductive dissolution of graphene, and other nanocarbon materials, a detailed description is provided elsewhere[78,80].

5.3 Exfoliation mechanisms

Exfoliation of graphite in a liquid can be achieved through various routes. The fundamental mechanisms used in most of the current top-down exfoliation techniques, can be broadly divided into three main areas. These principal mechanisms are mechanical, chemical and electrochemical. Mechanical exfoliation methods are typically non-oxidizing, meaning the graphene is produced without functionalisation of oxygen groups that can adversely impact electronic properties. Electrochemical exfoliation methods may, in certain circumstances, have an indirect oxidising effect.

The level of oxidation (i.e. C/O ratio), however, is limited compared to strongly oxidizing chemical approaches which often require post-processing reduction steps to improve material properties.

5.3.1 Mechanical exfoliation

Mechanical exfoliation relies on the use of force to break the van der Waals attraction between the planes in graphite. There are essentially three ways to overcome this attraction [84]:

1. Peel two graphite layers apart by applying a normal force to overcome the van der Waals attraction.
2. Application of a lateral, or shear force. Adjacent layers within graphite can slide in the lateral direction, when a suitable force is applied to overcome the van der Waals attraction.
3. Use exfoliation with fragmentation to break-down large graphite layers into smaller sizes. If the desired product does not require graphene of large area, then the method promotes easier exfoliation due to lower van der Waals interaction forces that are split across smaller sized graphite flakes.

5.3.2 Chemical exfoliation

Chemical exfoliation techniques utilise chemical approaches to turn the starting graphite into a graphite derivative. This can then be readily delaminated to give single or few layer sheets of chemically derivatized graphene. This derivative can receive subsequent treatment to convert it back to graphene. The most common of these techniques is the graphite oxide route, which capitalises on strongly oxidising graphite to produce graphite oxide. There are many approaches that have been developed for the preparation of graphite oxide. The Brodie method was developed using fuming HNO_3 and $KClO_3$ as intercalants and oxidants [85]. Hummers and Offeman proposed a method in which H_2SO_4, $NaNO_3$ and $KMnO_4$ were used. This method eliminated some of the hazardous steps that were present. However, the key issues still limiting the adoptability of this method includes the formation

of toxic gases such as NO_2/N_2O_4, difficulty in extracting out Na^+ and NO_3^-, and low conversion of graphite to graphite oxide [85].

The mechanism for the formation of graphite oxide, and subsequent treatment in solution to form graphene oxide, can be seen in Figure 10. Graphite is first oxidised using strong oxidants and with further hydrolysis, graphite oxide can be separated to give graphene oxide.

FIG 10

The chemical exfoliation process affects the final graphene oxide product by generating irreversible defects on graphene sheets during the oxidation process. This makes it insulating due to the disruption of graphitic networks. Graphene oxide then needs to be reduced to remove the oxygen functional groups, making it useful for electronic applications [86]. The final quality of the reduced graphene oxide, therefore, is dependent on the experimental parameters that are applied in the reducing step. The number of defective sites is nonetheless often – though not always – higher in rGO compared to other forms of graphene [87]. There are various reduction methods that are available in the literature for making rGO. The main ones include chemical reduction and thermal reduction. Other techniques such as solvothermal, photocatalytic, biomolecules, natural agents and plasma assisted reduction have also been explored. Table 2 summarises some of these techniques with the milestones achieved within the field. It is important to note that thermal reduction has been proven to give the best quality rGO with highest structural quality, as indicated by the high conductivity obtained in contrast to other techniques as shown in Table 2. It is also noted that it is possible to achieve a thorough conversion of graphene oxide into graphene sheets with heat treatment of above 1773 K[88].

This review focuses on liquid-phase methods that produce graphene without strong oxidation effects. Other reviews from Park and Ruoff[89], Genger *et al.*[90] and Thakur and Karak[91] provide further details on the chemical exfoliation route and environmentally friendly graphene oxide reduction methods.

Table 2: List of the reduction methods of graphene oxide along with key features of the resulting reduced graphene oxide. Reproduced with permission from ref. [92]. Copyright 2015 Elsevier B.V.

GO reduction methods	Reduction processes	C/O ratio	Electronic properties	
			Mobility (cm^2 V^{-1} s^{-1})	Conductivity (S/m)
Chemical reduction	Hydrazine	10.3[b]	-	2420
	Phenylhydrazine	9.5[b]	-	4700
	NH_3-BH_3	9.8[a]	-	20300
	55% HI acid	12.0[a]	-	29800
	HI-AcOH	11.5[b]	-	30400
	Ethylenediamine	7.8[a]	-	220
	Na-NH_3	16.6[a]	123 (hole)	-
	Nascent hydrogen (Al/HCl)	21.1[b]	-	12530
	HI + trifluoroacetic acid	10.5[a]	250 (hole) 200 (electron)	-
	Zn/HCl	33.5[a]	-	15000
	Thiourea dioxide/NaOH	14.5[a]	-	-
Thermal reduction	700 °C, H_2, 30 min	28.6[a]	-	8100
	1000 °C, H_2, 1 h	-	5.4 (hole) 1.1 (electron)	76000
	1000 °C, C_2H_2, 30 min	50.2[a]	-	143000
Plasma-assisted reduction	CH_4 plasma, 700 °C, 20 s	9.2[a]	-	34500

	Ar/H_2 plasma, 150 °C, 30 min	7.0[a]	-	-
Photocatalytic reduction	Polyoxometalate cluster ($H_3PW_{12}O_{40}$)	-	0.03 (hole) 0.01 (electron)	120
Solvothermal reduction	DMF + 0.6 M H_2SO_4, 1 h	8.4[a]	-	1223
	H_2O:NMP (1:1), 200 °C, 24 h	5.2[a]	-	374

a Obtained via X-ray photoelectron spectroscopy.

b Obtained via elemental analysis.

5.3.3 Electrochemical exfoliation

Unlike methods that rely on harsh solvents or oxidants, electrochemical methods take advantage of graphite's conductive properties to intercalate molecules between the graphene layers and therefore trigger exfoliation. Using graphite as an electrode, a positive or negative charge can be imposed on the material, promoting intercalation of oppositely charged ions and facilitating exfoliation. The mechanism for this process is illustrated in Figure 11 [93]. Oppositely charged species enter between the sheets, expanding them, and reducing the exfoliation energy. Through application of either mechanical based processes or sonication, the sheets can be separated in solution.

FIG 11

5.4 Exfoliation methods

The following methods have demonstrated liquid-phase exfoliation of graphite into graphene with minimal or no adverse oxidative effects. The number of novel top-down methods is continually growing and, therefore, the list presented below is not intended to be exhaustive. It contains, however,

a diverse range of common approaches that are relevant within the chemical engineering community. A brief summary of each approach is laid out in this section.

5.4.1 Solvothermal route

High-quality graphene can be produced at high-yield through a solvothermal process. This is a relatively simple, few-step process, to produce monolayer and few-layer graphene. Graphite flakes are dispersed in an organic solvent, acid or other suitable solvent that could effectively penetrate through the interlayers and heated at elevated temperatures (from several hundred degrees Celsius to a range of 1000-2000 °C).

Qian *et al*. [26] produced monolayer and bilayer graphene by solvothermal-assisted exfoliation. In the first process step, expandable graphite was heated to 1000 °C under a controlled atmosphere (95% of Ar, 5% of H_2) to enlarge the spacing between graphene sheets (Figure 12 a) and b)). The expanded graphite was then mixed with a highly polar organic solvent, acetonitrile, in a Teflon-lined autoclave (without adding any surfactants or stabilisers). The mixture was heated for a period of 12 h at 180 °C (Figure 12 c)). During this process, the acetonitrile molecules gained sufficient energy to overcome the potential barrier present in the expanded graphite interlayers and diffuse into them. After that, the mixture was sonicated, resulting in monolayer and bilayer graphene sheets (Figure 12 d)). Finally, centrifugation was used to obtain monolayer and bilayer graphene with a yield of 10 to 12 wt% at 600 rpm (Figure 12 e)). Separation of monolayer and bilayer graphene from expanded graphite was achieved by tuning the centrifugation velocity. The mixtures labelled by 1 to 4 in Figure 12 e) correspond to samples obtained using the process and centrifugation conditions stated in Table 3. More intense centrifugation enhanced the proportion of monolayers. This was accompanied by a reduction of the yield from ~12 wt% to ~1 wt%. The lateral size of the graphene sheets was shown to be widely distributed, ranging between 100 to 800 nm. Insignificant structural defects, such as scrolling and folding, were observed in the bilayer product. Otherwise, electron diffraction and Raman spectroscopy confirmed that the graphene produced was defect-free.

FIG 12

Table 3: Production metrics (or yield) for different types of graphite and exfoliation conditions. Reproduced with permission from ref. [26]. Copyright 2009 Tsinghua University Press and Springer Berlin Heidelberg.

Sample number (see Figure 12 e)	**Carbon source**	**Process**	**Centrifugation conditions**	**Yield (wt%)**
1	Expanded graphite	Solvothermal-assisted process	600 rpm, 90 min	10-12
2	Expanded graphite	Solvothermal-assisted process	2000 rpm, 90 min	0.8-1
3	Expanded graphite	Without solvothermal-assisted process	600 rpm, 90 min	None
4	Sieved graphite powder	Without solvothermal-assisted process	600 rpm, 90 min	0.5-0.6

Al-Hazmi *et al*. [94] produced graphene using a solvothermal process by mixing graphite flakes with tartaric acid followed by a short (60 s) thermal shock at 750 °C to expand the graphite. This mixture was hydrothermally treated with isopropanol at 400 °C for 120 min in a Teflon-lined autoclave. The autoclave was then quenched in an ice bath, and the product was appropriately filtered and left to dry overnight at 60 °C. Raman spectroscopy revealed that graphite was successfully expanded after the thermal shock, and subsequently, graphene sheets with low defects and oxidation degree (D to G intensity ratio of 0.06) were produced. The 2D/G intensity ratio was found to be around 2.3, indicating the presence of monolayer graphene sheets. Using 100 graphene sheets as a sample size, it was estimated that ~95% of the graphene sheets had an average thickness of 0.53 ± 0.04 nm (monolayer), while ~5% had an average thickness of 0.75 ± 0.05 nm (bilayers). The lateral dimensions were found to be distributed between 250 and 450 nm. Finally, X-ray photoelectron spectroscopy (XPS) showed that the final graphene sheets contained ~6% oxygen.

Liu *et al*. [46] prepared graphene sheets with 2-6 layer thicknesses in an ethanol solution by the solvothermal route, and reported several important findings. Firstly, increasing temperature in this process removes oxygen-containing groups, and better quality graphene sheets are obtained by essentially restoring π-bonding. Secondly, the D to G intensity ratio increases as the solvothermal temperature rises. This could be explained by the formation of defects upon removal of oxygen atoms at increasing temperatures. TEM characterisation showed previously observed structural defects such as curled and partially-folded structures. HRTEM revealed the presence of graphene sheets with various thicknesses that are in the range of 2 to 6 layers.

Further information can be found in a review by Sasikala *et al*. [95] which takes an in depth view of solvothermal processing, including how the synthesis condition affects the morphology and band properties of the materials obtained.

5.4.2 Microwave irradiation

Microwave irradiation is another example of thermal exfoliation of graphite. This approach is typically faster than the solvothermal route and has been reported in a number of papers. For instance, microwave irradiation in ionic liquids was investigated by Matsumoto *et al*. Using this method, graphite was dispersed in an ionic liquid and irradiated with microwaves for 30 min (Figure 13). The set-up is somewhat similar to ultrasonication, but the processing time is greatly reduced, and an improved route for graphene exfoliation was demonstrated. The authors reported a high exfoliation efficiency, a yield of 93 wt% and a selectivity of 95% towards single-layer graphene [24]. The D/G ratio measured by Raman showed a value of ~0.14 (similar to the precursor graphite with value of ~0.13), demonstrating a high-quality graphene product. The authors suggested that HF species, generated under microwave irradiation by partial decomposition of the fluorine-containing ionic liquids, play a crucial role in the exfoliation. Sterically less-demanding HF molecules first intercalate stochastically into the thermally agitated interlayers of graphite. This produces structural disordering of the graphite,

and promotes intercalation of the sterically more-demanding ionic liquid molecules with enhanced affinities. This effect is attributed to the splitting of graphitic layers [24].

FIG 13

Liu *et al*. [96] demonstrated a fabrication method of multi-layer graphene flakes produced with an increased exfoliation efficiency through intercalation and decomposition of H_2O_2 and $(NH_4)_2S_2O_8$. Starting with commercially available expandable graphite, firstly, they have processed it for 10 seconds using microwave heating before mixing and intercalation individually with the above-mentioned compounds. It is reported that intercalation begins to occur at the defect and edge sites as well as grain boundaries. Once these compounds start to decompose into various gases e.g. oxygen and steam, this leads to an increase in the graphite interlayer distance allowing even more molecules to participate in the intercalation. Subsequently, this results in an effective expansion and exfoliation of graphite in the process of second microwave heating. This mixture is then sonicated and centrifuged to obtain a stable dispersion of graphene sheets, which was then used for characterisation. AFM images showed that the mean thickness of multi-layer graphene sheets prepared in H_2O_2 was about 6.15 nm with lateral sizes reaching several micrometers, whereas multi-layer graphene sheets prepared in $(NH_4)_2S_2O_8$ had larger mean thickness of approximately 9.15 nm. Raman spectroscopy have showed that values for both the I_D/I_G and I_D/I_{2D} are noticeably lower for each mixture compared with precursor and initially heated graphite materials. This demonstrates that further heating by microwaves allows to restore crystalline quality. FTIR spectra showed that graphene product prepared in H_2O_2 has much less oxygen-containing functional groups than the graphene product prepared in $(NH_4)_2S_2O_8$. This may occur due to the fact that oxide radicals are released as ammonium persulfate decomposes, which initiate radical induced cutting along the edges and surface defects.[97] Similarly, Liu *et al*. [98] have fabricated high-quality graphene sheets which had lateral size of up to 100 µm and thickness of just few layers. Comparing to the conventional Hummer's method [99] , this research group claims that their prepared graphene sheets are on average 10 times larger in size. Moreover, in their graphene fabrication process, no post-processing such as ultrasound, centrifugation, shock or H_2O_2

treatments are required. They used commercial expanded graphite and applied microwave irradiation for 10 seconds, following which the volume of this graphite powder expanded dramatically. It was then mixed with concentrated sulfuric acid and $KMnO_4$, where the reactant ratio of $KMnO_4$ to expanded graphite was set to 2:1. The whole mixture was then further heated by microwave radiation for further 10 seconds. This processed powder was characterised using SEM and TEM which proved to contain transparent, continuous, wrinkled and agglomerated microstructures of graphene sheets. As characterised by AFM, prepared graphene-oxide sheets had lateral dimensions of about 50 µm and mean thickness of approximately 2.15 nm (but ranging between 1 and 12 nm). Analysis by XPS showed that the produced graphene oxide sheets have C/O ratio of 2.6. Structural properties were probed using Raman spectroscopy, which confirmed the intensity ratio between D and G bands (I_D/I_G) to be 0.85. Oxygen-containing functional groups were identified using FTIR, and the results clearly showed the effectiveness of deoxygenation/reduction by the final microwave heating step. Comparing oxidized and intercalated graphite powder with the final microwaved graphene sheets, it is evident from the spectra that the latter has much weaker peaks than both the former and precursor materials.

Another interesting work was conducted by Lin *et al.*[100], where the group used ammonium bicarbonate as the intercalation product (without the addition of solvents) in the microwave-assisted exfoliation of graphite. This graphene production method, which involved pristine graphite and ammonium bicarbonate agitation, thermal treatment and microwave irradiation, produced 5-8 layers graphene sheets with lateral sizes of 0.4-0.8 µm as characterised using AFM. Evidenced by TEM, the edges of the produced graphene sheets were partially folded and had wrinkled surfaces. Moreover, the presence of graphene in the final product was confirmed by XRD and Raman spectra. Analysis performed using XPS revealed that the O/C ratio was 0.168, meaning that only several oxygen-containing groups were attached to graphene sheets. According to Tang *et al.* [101], ammonium bicarbonate acts as an effective dispersant in graphite powder and prevents graphene from agglomeration. It also attaches to the edge defects of graphite by heating and cooling treatment of this mixture. Thermal decomposition of ammonium bicarbonate leads to formation of various gaseous

species (e.g. CO_2, NH_3, H_2O) which can overcome graphite interlayer van der Waals forces and subsequently, results in effective exfoliation of graphite.

5.4.3 Supercritical Fluids

The use of supercritical fluids has also been extended to exfoliating graphene sheets. The critical factors to consider using this technique are the high diffusivity, expansibility and solvating power of the supercritical fluid. The supercritical fluid can penetrate the gap between the graphite layers owing to the high diffusivity and low viscosity of the supercritical fluid. Once a rapid depressurisation happens, the supercritical fluid will abruptly expand to predominately generate a normal force for exfoliating graphite as seen in Figure 14 a).

Pu *et al*. used supercritical CO_2 gas to exfoliate graphite in a solution containing a sodium dodecyl sulphate dispersant. Graphene flakes of typically 10 atomic layers in thickness were obtained [47]. In a different study, Rangappa *et al*. used supercritical ethanol, NMP and DMF for the exfoliation [102]. The solvents were heated up to, or above, their critical temperature and the exfoliation of few-layer graphite (<10 layers) was achieved in the shortest reaction time of 15 min. Approximately 90–95% of the exfoliated sheets were less than 8 layers with approximately 6–10% monolayers [102].

FIG 14

An attempt to scale-up graphene production using shear-assisted supercritical CO_2 exfoliation was reported by Li *et al*. [43]. The experimental apparatus is shown in Figure 14 b). In all experiments, the process time was fixed at one hour. When CO_2 fluid with graphite powder is subjected to a high shear stress, graphite flakes expand and delaminate into multilayer graphene sheets. Temperature was found to be an important factor as it directly affects the graphene yield. An increase in temperature from 35 to 55 °C, subsequently increased graphene yield from 40% to 87%, when other parameters were kept constant. This is due to the enhanced energy kinetics of the CO_2 molecules and therefore thermal motion. It was also observed that higher pressure slowly increased exfoliation yield. This trend is related to the larger quantity of CO_2 molecules at high pressure that can penetrate the interlayer space

of graphite. The effect of the mass of graphite on the exfoliation process was also investigated. The study showed that increasing the amount of graphite by 95wt% lowered the exfoliation yield from 80% to 40%. This is due to an insufficient CO_2/graphite ratio causing smaller shear stress. Rotational speed was another parameter investigated. It was found that increasing rotor speed from 0 to 2000 rpm, increases the exfoliation yield from 10% to 70%. The main driver of this is an increase in turbulent shear stresses in the mixture, which overcomes the van der Waals force barrier with a greater effect than at lower rotational speeds and they were able to obtain 90% exfoliated sheets with less than 10 layers, and 70% between 5 and 8 layers [43].

Recently, the combination of supercritical fluid and sonication was reported by Gao *et al*. [17]. In this study, graphene flake distributions were 24% monolayers, 44% bilayers, and 26% trilayers. Song *et al*. [103] investigated a fluid dynamics method in supercritical CO_2. Scale-up of graphene production was attempted by combining two exfoliation mechanisms to increase the yield. A shear method, coupled with the expanding CO_2 exfoliation method, was implemented. This approach led to a yield of ~63% with a selectivity of monolayer graphene of 27%. Overall, a major challenge of the supercritical fluid method is the need for pressurised reactors to facilitate the process. For example, the work of Gao *et al*. [17] required pressures of 12MPa to achieve the above stated yields.

5.4.4 Vortex fluidic device

Another shear-driven process to exfoliate graphite in an organic solvent was developed by Chen *et al*. This approach employed a rapidly rotating tube to generate an intensive shearing environment for the production of graphene from graphite [104]. A schematic of the set-up is shown in Figure 15. A thin liquid (i.e. NMP) film was created when a glass tube was set to rapidly rotate at an angle varied between 0° and 90°. High internal shear stresses within the thin liquid film provided the necessary conditions for exfoliation. The balance between gravitational and centrifugal forces was adjusted, by varying the previous parameters, to examine the impact on exfoliation performance. A rotational speed of 7000 rpm, an inclination angle of 45°, and a processing time of 30 min were found to be the

optimal settings for graphene exfoliation. TEM characterisation established the yield of the graphene sheets to be ≤ 1 wt%. The yield of monolayer graphene sheets depended on the morphology of the precursor graphite flakes (i.e. size, chemical and physical properties of the edges), and the orientation and magnitude of the shear force. Selected Area Electron Diffraction (SAED) confirmed a hexagonal distribution of peaks for graphene, and AFM height profile measurements were approximately 1 nm.

It was proposed that Stewartson/Ekman layers are formed by liquid flowing downwards close to the gas-liquid interface, and liquid flowing upwards close to the wall of the rotating tube (Figure 15 c)). In the rapidly rotating fluid, the shear layers are parallel to the axis of rotation. The large centrifugal force initially accelerates graphite flakes to the walls of the tube. For a tube rotating at 7000 rpm and inclined at an angle of 45^{o}, this produced an average liquid film thickness of approximately 230 μm. The average thickness of the flakes was less than 1 μm. Chen *et al*. suggested that the flow rate above the flakes is close to the maximum [104]. The mechanisms shown in Figure 15 d) and e) for graphite layer-by-layer exfoliation in a thin film were supported by the partially stacked graphene sheets observed using TEM. The exfoliation involved a slippage process, where the graphene sheets are displaced relative to each other. This requires lifting individual sheets from the surface of the bulk graphite through the presence of lateral force. Graphene sheets were found to be attached to the walls of the tube, suggesting that this slippage of graphene sheets can also occur on the surface of the tube. A large centrifugal force can, therefore, hold the graphite flakes against the internal tube wall and simultaneously provide a shear-induced displacement along the surface.

FIG 15

Wahid *et al*. [105] used a similar vortex fluidic device, and experimental parameters to those developed by Chen *et al*. [104], in an attempt to produce a graphene hybridised material with algal cells for use in the removal of nitrate from liquid effluents. Firstly, graphite was dispersed in water and exfoliated into multi-layer graphene using a vortex fluidic device at the optimal operating conditions that created the required environment for intense shearing. Materials characterisation using SEM, TEM and AFM

indicated the presence of multi-layer graphene sheets. The multi-layer sheets had varied thicknesses, some thicker than 20 nm and a small portion of ~1 nm thick flakes. The characteristic peaks from Raman spectroscopy indicated that the graphene sheets were ≥ 5 layers thick and contained similar defects to those present in precursor graphite flakes. Hence, the results obtained from the different characterisation techniques imply that the vortex fluidic device can only produce multi-layer graphene when operated at the optimal parameters (i.e. 7000 rpm and 30 min processing time). It may be possible to thin-out these layers closer to monolayer sheets if processing time was prolonged. This, however, would offer a less practical approach towards mass-scale graphene production. The approach is less energy intensive than sonication and offers a more feasible approach for the scale-up graphene production.

5.4.5 Taylor-Couette device

Tran *et al*. [106] demonstrated that a high shear environment, created in a Taylor-Couette flow reactor, could be used to exfoliate graphite flakes with a relatively high yield. Graphite flakes, dispersed in a stabilising solvent (NMP), were processed using this method. The liquid suspension flows through a small gap between a rapidly rotating inner cylinder and stationary outer cylinder (Figure 16). Once the inner cylinder is rotating above a critical rotational speed, a secondary flow occurs which is distinguished by the presence of counter-rotating toroidal vortices, also known as Taylor vortex flow. A sufficient local shear stress at the reactor wall was created, leading to the exfoliation of graphite flakes into graphene sheets with a low degree of defects.

FIG 16

The graphite/solvent dispersion was continuously recirculated through the reactor and a separate chiller (to prevent heating of the mixture) for 10 min to 120 min. Rotation of the inner cylinder was varied from 500 rpm to 3000 rpm. The mixture was centrifuged and the exfoliated graphene in the supernatant was collected for characterisation. SEM images were used to observe graphene sheets which were thinner than the precursor graphite flakes. Variation in flake lateral sizes were between 500 nm and 1500 nm (as observed from TEM images). This size distribution potentially indicates

that a fragmentation mechanism occurred in the exfoliation process. This could also be due to the wide particle size distribution of the graphite precursor. An electron diffraction pattern confirmed the presence of graphene monolayers. AFM images confirmed the values of the flake size and showed that most of the flakes were less than 3 nm thick, corresponding to few-layer graphene sheets. The thinnest sheets observed were 0.6 nm. A sample size of 250 flakes were also characterised by AFM to determine the height profile. This showed that over 90% of these flakes were less than five layers thick. A low degree of defects was evident with an I_D/I_G ratio of ~ 0.14. Furthermore, XPS showed that produced graphene sheets were not oxidised, confirming the high quality of these flakes.

5.4.6 Spinning disc processor

Using a spinning disc processor, Chen *et al*. generated a shear force in dynamic thin films across a disc surface. This led to the exfoliation of graphite flakes, and production of carbon nanoscrolls [107]. Hexagonal boron nitride (h-BN) scrolls were also produced using this technique. A schematic diagram of the spinning disc processor is shown in Figure 17 a). As illustrated in Figure 17 a), a jet feed of the suspension (i.e. graphite or h-BN flakes dispersed in NMP) is directed near the centre of a 20 cm diameter disc that has a grooved surface. Due to the high-speed of rotation (2500 rpm), the liquid spreads across the disc forming a thin film with high surface area-to-volume ratio. This speed results in a short residence time for the dispersed particles (< 1 s as noted in this paper). Hence, the 200 mL solution is recycled for over 20 h at 60 mL min^{-1} flow rate.

From the TEM images, carbon nanoscrolls (with approximate yield of 1%) were both multi-layered (exact nanoscroll thickness was not specified) and irregular in shape. Various sheet deformations were observed, shown in Figure 17 c). These deformations may have formed either due to high-velocity impact or the intense shearing environment. The impact occurs when particles leave the surface of the rotating disc, and strike the walls of the tank surrounding the disc. The irregular material shapes vary considerably in length and diameter, which could be due to a variation in the original graphite flake sizes. A significant number of partially formed carbon nanoscrolls were also observed.

This could be caused by the irregular morphology of the graphite flakes under varying localised micro-fluidic conditions. Chen *et al*. proposed a potential mechanism, illustrated in Figure 17 b). Particles, suspended in NMP, are immediately accelerated by the centrifugal force when introduced from the feed jet onto the surface of the spinning disc. The liquid suspension quickly spreads across the disc, forming a dynamic thin film typically ≤ 200 μm thick [107]. Suspended flakes move throughout the thin film, with periodic contact with the surface of the rotating disc. High shear forces occur from the viscous drag of the liquid on the surface of the disc and result in exfoliation. Grooves through entire surface of the disc, shown in Figure 17 a), may further enhance the frequency of the collisions of the flakes with the surface of the disc.

FIG 17

Analysing SEM images, the authors proposed three feasible scenarios for exfoliation occurring due to shearing (Figure 17 b)). The first two mechanisms may involve exfoliation of the bottom layers with different degrees of folding due to lift from the shear force on the upper layer of the flakes. The third mechanism may involve curving of the flake edges to form scrolls. Since these three mechanisms may compete with one another, their occurrence will depend on various factors such as flake orientation, nature of the material, number of layers exfoliated at once, shear intensity, etc. Molecular simulations for a single graphene sheet were also performed, and an analytical continuum model for the scrolling of the graphite flake provided an insight on the scroll formation.

5.4.7 High-shear mixing

High-shear mixing has been demonstrated in the literature as a potential method for scale-up of graphene production by Paton *et al*. [40]. Liu *et al*. used a high-shear mixer to exfoliate graphite and produce graphene flakes. The head of this mixer contained a rotor and a stator with an adjustable gap of between 100 and 3000 μm (Figure 18 a) and b)). When the rotor operated at high speed (10-50 m s^{-1}), high shear rates (20,000-100,000 s^{-1}) forced the suspension to flow through the narrow gaps between a rotor and a stator [41].

Liu *et al.* identified that the graphene sheet size and thickness can be controlled by setting a specific gap size between rotor and stator [41]. In fact, they have observed that a small stator produces smaller graphene sheets than the larger stator. Approximately 1000 flakes were analysed for average size and thickness to assess the effect of the gap size. Using a small stator, the graphene sheets had an average size and thickness of 0.35 µm and 0.9 nm, respectively. Those prepared by a large stator had an average size and thickness of 0.9 µm and 1.3 nm, respectively. Hence, higher shearing stresses (achieved by using small stator with narrower gaps between rotor and stator) are preferred to produce thinner and smaller graphene flakes relative to a larger stator with wider flow channels.

FIG 18

Similarly, the mixing effect on graphite exfoliation was also explored by Paton *et al.*, using a mixer with a rotor/stator head. TEM was used to measure the size of the nanosheets, found to be in the range of 300 to 800 nm. AFM images showed that the graphene sheets consisted of 10 layers and less. Raman spectroscopy confirmed the presence of graphene monolayers. The authors suggested that turbulent energy dissipation is not necessary to achieve effective graphite exfoliation. Production characteristics were assessed for varying rotor speed and rotor diameter. As shown in Figure 19 a), graphene was produced at both low ($Re < 10^4$) and high Reynolds number ($Re > 10^4$). Reynolds number was defined as $\frac{ND^2\rho}{\eta}$, where N is rotor speed, D is rotor diameter, ρ and η are the liquid density and viscosity, respectively. Graphene was produced at a minimum shear rate of 10^4 s^{-1} (Figure 19 a)) and within a laminar flow regime, supporting the suggestion that turbulent flow is unnecessary for exfoliation. Several possible mechanisms for graphite exfoliation were offered and are illustrated in Figure 18 c). These include shear force, cavitation and various types of collisions. Although the shear mixing method has demonstrated some of the highest production rates currently (i.e. 5.3 g/h), there may be limitations in yield and throughput, as the high shear rates are generated locally within a micron-scale rotor-stator gap.

Ultimately, it can be deduced that the same exfoliation mechanism occurs in both turbulent and laminar flow regimes. Any mixer, therefore, that can generate a shear rate of 10^4 s^{-1} and above, should be capable of producing graphene. Paton *et al.* demonstrated this using a kitchen blender, where local turbulent shear rates of more than 10^4 s^{-1} are generated by the rotating blade.

A more detailed work using a kitchen blender was performed by Yi *et al.* [108] to understand the viability of this process in the production of graphene. The process employed rapidly rotating mixer blades that create a high-shear region across a larger volume than that in the rotor/stator space. Although this high shear region is not localised, the shear rate decreases with increasing distance from the mixer blades. Hence, there is an opportunity to develop a high shear region across the whole mixing volume if suitable engineering design and optimal process parameters are applied. Once this is established, there are four exfoliation mechanisms that could occur within this region: (i) viscous shear stress induced by a velocity gradient, (ii) Reynolds shear stress induced by turbulent velocity fluctuations, (iii) graphite-graphite collisions due to high inertial forces that dominate viscous forces in turbulent regions, (iv) normal-forces caused by pressure differences that arise from turbulent pressure fluctuations.

FIG 19

Varrla *et al.* [109] extended the use of the kitchen blender to produce graphene by exfoliating graphite dispersed in a surfactant. AFM and TEM characterisation results showed that mono- and few-layer graphene sheets were successfully produced but contained some folded flakes. For this specific model of kitchen blender, an optimal blade rotational speed was identified to be around 2000 rpm. This was found by analysing graphene concentration produced under a variable blade rotational speed.

Both Yi *et al.* and Varrla *et al.* presented graphene flake size and thickness distribution using AFM results. Yi *et al.* set the rotational speed of the blade to 5000 rpm and performed the experiment for 8 h, collecting samples at regular time periods. Approximately 92% of flakes analysed were less than

1.5 nm thick. The fraction of flakes with ≤ 1 nm thickness was between 14.6% and 20% for all mixing times. It was also observed that longer processing times result in noticeable decreases in flake area (i.e. from ~ 2.4 μm^2 at 30 min to ~ 0.1 μm^2 at 8 h). These values can be compared with those obtained by Varrla *et al.*, where the rotation speed of 18000 rpm for 1 h was employed. The average sheet length and average layer number were 320 nm and 6, respectively.

5.4.8 Sonication

Sonication is a liquid-phase exfoliation technique that has been widely employed to produce graphene mono- and multi-layer sheets. The process typically involves a subsequent centrifugation step as a way to separate the residual graphite flakes from the exfoliated sheets. Sonication can be used either solely, or be combined with other techniques.

Exfoliation via sonication relies on the production of high intensity ultrasonic waves that travel through the liquid media at a specific frequency. Cavitation bubbles are produced, and grow to the order of microns in diameter. These bubbles become unstable and rapidly collapse during a high-pressure cycle as illustrated in Figure 20. These collapsing bubbles create hot spots where temperatures of ~ 5000 K, pressures of ~ 1000 atmospheres, and heating and cooling rates of more than 1000 K s^{-1} are reached [110]. These cavitation-induced bubbles distribute around the graphite flakes and when bubbles collapse, micro jets and shock waves can act on the graphite surface, producing compressive stress waves that propagate throughout the graphite body. From the theory of stress waves, once the compressive wave spreads to the free interface of graphite, a tensile stress wave will be reflected back to the body.

The collapse of numerous micro-bubbles will, therefore, lead to intensive tensile stresses in the graphite flakes. Two secondary processes are also possible. Unbalanced lateral compressive stresses can separate two adjacent flakes: (i) by a shear effect, and (ii) micro-jets may split the graphite flakes

just as a wedge is driven into the interlayer. All this implies that it is the tensile stress that effectively exfoliates graphite into graphene flakes, resulting in a normal force dominated mechanism [84].

FIG 20

Hernandez *et al.* [18] first reported high yield production of graphene via sonication. Graphite powder was dispersed in organic solvents such as DMF and NMP, followed by sonication and centrifugation. A graphene dispersion was obtained with a monolayer concentration of 28%. Although the set up and experimental method are relatively straight forward, other recent works showed that this method produces very low graphene concentrations, ranging from ~0.01 mg/mL to ~1 mg/mL [20]. Prolonging sonication time to around 1000 h, higher concentrations of graphene in dispersions (Figure 21) were achieved, but this becomes impractical due to excessive processing time and energy.

Further work was done to achieve high concentration by adding surfactants and polymers, solvent exchange methods, and mixing solvents[44,45,49,52,56,73,111-115]. All the methods within these studies are still plagued with the main drawback of low rate of graphene production and long processing time. In addition, the exposure of graphene particles to a high energy sonication environment also reduces flake size and increases the level of surface-edge defects [44]. Further development in this area is required in order to comprehend all the variables involved i.e. vessel geometry, position of the sonication probe, optimal sonication parameters under given conditions, solvents and surfactants safe for the health and environment, etc., and how these can maximise graphene production with the minimum number of defects. Alternatively, more development works could be performed by combining ultrasonication with other graphene exfoliation methods i.e. fluid-dynamics. We note three recent reviews by Lavin-Lopez *et al.*, Ciesielski and Samori, and Muthoosamy and Manickam which expand into more detail on the topic of exfoliation via sonication [116,117,118].

FIG 21

5.4.9 Jet cavitation

Jet cavitation is another method that has been developed to capitalise on the effect of shearing. Liu *et al.* [119] found that jet cavitation can be induced with a high pressure difference in a cavitation generator (Figure 22 a)). Similar to the sonication method, the collapsing bubbles provide a mechanism for exfoliation of graphite into few layer graphene flakes. The system consists of multiple flow channels where the exfoliation occurs at various positions due to pressure differences between the inlet and the outlet. A continuous flow of graphite/solvent dispersion was injected to the pressure vessel and pressurised by a plunger pump. As illustrated in Figure 22 b), this created many bubbles, an upon imploding, created micro-jet and shockwave forces across the graphite surface. This mechanism produced graphene flakes, and is described in detail in Section 5.4.8. AFM showed that graphene flakes had a height range of approximately 0.8 – 0.9 nm. The HRTEM showed the presence of few-layer graphene sheets.

The exfoliation of graphite is also driven by other mechanisms i.e. turbulence-induced Reynolds shear stress, viscous shear stress, pressure release and collisions of graphite particles with one another as well as channel walls, induced by turbulence. These mechanisms lead to lateral-, normal- and shear-force dominated exfoliation as well as fragmentation.

FIG 22

Liang *et al.* [23] produced graphene nanomesh (i.e. sheets with a porous structure) using a similar fluid-based device to that of Liu *et al*. An analysis of the flake distributions was conducted on 100 flakes collected from several AFM images. Over 70% of the flakes were 1 to 1.5 nm thick, with the remaining less than 1 nm thick. A minor amount were observed to be thicker than 1.5 nm. Liang *et al.* have illustrated several exfoliation mechanisms of this scenario. Liang *et al.* [120] also highlighted that the variation of the treatment time and pressure directly affects thickness, lateral size and concentration of graphene by jet cavitation. As the treatment time is increased, there is a shift of thickness distribution to a lower and narrower range of values. The total amount of graphene flakes

with a thickness of less than 1.5 nm increases from 29% after 30 min treatment, to 63% after 4 h treatment, and 79% after 8 h treatment. The same applies for the flake area, where the values drastically change from a wide distribution after 30 min treatment to a narrow distribution after 8 h treatment with 85% of the exfoliated flakes having $< 10^5$ nm^2. Prolonging treatment time and applying higher pressure also have a positive effect on the graphene yield.

5.4.10 Chaotic flow with sonication

Liu *et al.* [42] performed liquid exfoliation of graphite in NMP (initial concentration 6 mg mL^{-1}) by so called chaotic flow followed by sonication. This suspension was placed into a sample holder of the chaotic flow apparatus. Within the sample holder there were four cylindrical ceramic pebbles that lead to particle-pebble and graphite inter-particle collisions. Chaotic flow is created through rapid separation of liquid streams around these pebbles. Liu *et al.* proposed two mechanisms that most likely occur during this exfoliation process. The first one is the high-shear environment that is created between the suspension and the pebbles. The second mechanism may occur due to the formation of curled-up edges of the graphite crystal. After some time, these separate from the graphite flake by a collision-induced force and are dispersed in the NMP as exfoliated flakes. Approximately 0.034 mg mL^{-1} of graphene was produced after 2 min. Yield was increased to 0.11 mg mL^{-1} by prolonging the chaotic flow process to 30 min. Centrifugation was followed by re-dispersal of the top 80% supernatant in NMP. This solution was then sonicated. This two-step exfoliation process resulted in higher concentrations over time compared to direct sonication. A graphene sheet (GS) concentration of 0.430 mg mL^{-1} was reached after 8 h of sonication for the combined treatment compared to 0.119 mg mL^{-1} for pure sonication (8 h). These concentrations also appear typical for other sonication only studies, as seen in Section 5.4.8. Using AFM and TEM characterisation, a significant number of exfoliated flakes had a lateral size below 1 μm and in the range of several hundred nanometers. AFM indicated that the thickness of exfoliated flakes was in the range of 0.5 and 1.8 nm, suggesting that the graphene sheets were ≤ 3 layers. Raman spectroscopy showed a slightly higher value of ≤ 5 layers

thick. An advantage of this method is the reduction in processing time. One of the main drawbacks of this process, however, is the low yield (< 10%) of graphene from the initial graphite concentration.

5.4.11 Electrochemical exfoliation

The electrochemical exfoliation process utilises the electrical conductance of the graphite precursor, to apply a positive or negative charge on the material. This mechanism is shown in Figure 11. Oppositely charged ions, intercalate the graphitic electrode and induce exfoliation. The most common intercalating species include halogens, alkali metals, metal halides and various acids. In electrochemical exfoliation, the main components of the experimental set up include: a graphite working electrode, a counter electrode, a reference electrode, an electrolyte and a power supply. Graphite flakes are normally adhered to carbon tapes to improve its conductivity as a working electrode. A typical experimental set up is shown in Figure 23 a). The working electrode and counter electrode are immersed into an electrolyte with a certain distance kept between them. A positive (anodic electrochemical exfoliation) or negative (cathodic electrochemical exfoliation) voltage is applied to the graphite working electrode, depending on the desired exfoliation mechanism.

Liu *et al.* [121] utilised two pencil cores as graphite sources which acted as both the anode and the cathode. An alternating bias between +7 V and -7 V was used to exfoliate them. However, this led to inhomogeneity in the thickness and size distribution. Abdelkader *et al.*[122] proposed a novel system to turn the process to a continuous operation as can be seen in Figure 23 b). In this untested concept, it was proposed to insert the graphite from the bottom, and areas in contact with the electrolyte would be exfoliated. Liu *et al.* combined the use of ultrasonication and electrochemical exfoliation simultaneously [55]. It was found that the selectivity of thinner layers of graphene was obtained by introducing sonication.

Anodic Exfoliation

This method was initially used to produce acid salts of graphite since the 20th century. Interestingly, this substance can form graphene flakes by applying high temperatures [123]. Parvez *et al*. used a series of inorganic salt aqueous electrolyte solutions in anodic exfoliation, and demonstrated that sulphate ions have the highest exfoliation energy. A yield of 75 wt% was achieved when the concentration of the anions was 1 M. The Raman D/G intensity ratio was about 0.25 [25]. A mechanism was proposed for this process in which the production of hydroxide ions (i.e. strong nucleophile) occurs. These ions interact with the sp^2 carbons at the graphite edge, and further interactions with hydroxide ions result in the formation of an epoxide ring. This aids the expansion of the graphite layers, allowing the intercalating species such as sulphate ions, to promote exfoliation. The production of side gases, O_2 and CO_2, has also been reported to play a role in the exfoliation process.

Many researchers have attempted to optimise this technique to mass-produce graphene efficiently using different electrolytes such as: sodium dodecyl benzene sulfonate as the electrolyte [124], poly(sodium-4-styrenesulfonate) solution [50], copper phthalocyanine tetrasulfonic acid [125], 6-amino-4-hydroxy-2-naphthalene-sulfonic acid in a mixture of sodium hydroxide as the electrolyte [126]. These various routes have produced different types graphene from mono-layer to MLG. The disadvantage of this method is that there may be oxidative functional groups that bound to the surface of the product, which may subsequently affect the final properties of the graphene obtained.

The advantage of high yield with low production times that anodic electrochemical exfoliation offers is strongly hindered by the production of graphene oxide. A lower oxygen content is, however, possible in comparison to normal rGO with the O/C atomic ratio (atomic oxygen to carbon ratio) ranging from 0.10 to 0.20 [127]. Several researchers have tried to address this issue and a review by Paredes *et al*. [127] details some of the approaches that have been taken.

By tailoring the electrolyte or introducing additives to the solution, it has been shown by various researchers that the O/C atomic ratio can be minimised whilst maintaining efficient exfoliation. It has been found that the key issue with the process arises from the formation of oxygen radicals (e.g. ·OH)[127]. Most of the strategies adopted, therefore, have aimed to minimise the effect of such radicals in the intercalation process. The use of an equimolar proportion of glycine and H_2SO_4 was investigated by Rao *et al.* [128] and it was found that the O/C atomic ratio was 0.12. It was further improved by Chen *et al.*[129] using melamine instead and obtained O/C atomic ratio of 0.04. Hossain and Wang [130] investigated the use of H_2O_2 in the electrolyte and reported low oxidation. Reducing agents such as 2,2,6,6-tetramethylpiperin1-yl oxyl (TEMPO) was used successfully by Yang *et al.* [131] to get an O/C atomic ratio of 0.04 and I_D/I_G ratio of 0.1

FIG 23

Cathodic Exfoliation

In anodic exfoliation, the electrochemical exfoliation potential is greater than the oxidative potential. Hence, the graphene formed usually has oxidative species attached to it which affects its electronic structure. To circumvent this issue, researchers have tried to exfoliate graphene using it as the cathode electrode instead which reduces the extensive oxidation of graphene resulting in a structurally better product. Research in this field came from past applications of graphite when it was used as the negative electrode in lithium ion battery technology. Lithium can act as an intercalation agent and form lithium hydroxide, freeing graphene sheets when the graphite-lithium intercalated compound decomposes in water [123]. A disadvantage with this technique is the slow kinetics, and many researchers have tried to optimise the process to overcome this problem.

To improve the kinetics of the process, Huang *et al.* used molten LiOH/ LiCl at 600 ºC, but failed to achieve complete exfoliation of graphite and needed sonication steps to achieve sensible yields [19]. Zhong and Swager [132] proposed using Li^+ (from lithium perchlorate electrolyte) followed by tetraalkylammonium in two steps, however, a technical issue arising from the high ohmic drop created

by the electrolyte, required high potential and still needed sonication treatment afterwards. Abdelkader *et al*. proposed a method using DMSO due to its intrinsic property of having a wide electrochemical window, whilst being an effective solvent to form graphene. The DMSO electrolyte contained triethylammonium and Li ions to produce large flakes of about 20 µm lateral size. This setup also had the additional benefit of producing SO_2/ ammine gases that apply enough stress via expansion between the sheets to overcome the van der Waals attractions [122]. Yang *et al*. used N-butyl, methylpyrrolidinium bis(trifluoromethylsulfonyl)-imide and claimed to get graphene sheets between 2-5 layers that were free of defects [29]. Yang *et al*. also claimed to get pure cathodic exfoliation that did not require additional steps after using N-butyl, methylpyrrolidinium bis(trifluoromethylsulfonyl)imide ionic liquid but required potentials in the excess of -30 V [29].

Cooper *et al*. reported promising results using this technique. A tetralkylammonium salt was used in NMP as the electrolyte, and produced purely cathodically exfoliated material with a low voltage of -2 V for approximately 48 h. The resultant graphene consisted of mainly 2-5 layers (thickness of 1.8 nm), exhibited some defects as indicated by the I_D/I_G of 0.64, and did not contain any signs of oxidation [53].

Shear-assisted electrochemical exfoliation

Although electrochemical methods can exfoliate graphite into graphene, many issues arise from this technique. In the case of anodic exfoliation, the oxidation of the graphene has a significant effect on the quality produced. The slow kinetics in cathodic exfoliation limits its scalability in industry. Shinde *et al*. proposed a combination of two mechanisms to efficiently exfoliate graphite [54]. Applying minimal anodic potential, the oxidative effect was reduced. Simultaneously applying shear promoted the graphite expansion with intercalation of sulphate ions between the individual graphene sheets. A schematic of the micro-reactor in this experiment can be seen in Figure 24 a). The effect of applying various levels of shear with electrochemical exfoliation was investigated and the outcome of this is presented in Figure 24 b). Above 4 V, the process is electrochemically dominated. Below that voltage,

the effect of the coupled interaction of the two mechanisms is evident. At the lowest voltage potentials (1-2V), the process is shear dominated. Under the applied shear, an initial expansion of the graphene sheet due to the intercalated molecules could have enhanced exfoliation. Mono- and bi-layer graphene was produced using this method and confirmed with AFM measurements. The potential applied played a pivotal role in determining the selectivity of the number of layers. At a low potential of 1 V, the average thickness of the graphene sheet was below 4 layers (less than 75%). In contrast, applying a 5 V potential resulted in thicker layers (5-6). Shinde *et al*. noticed that increasing the potential from 1-10 V increases the I_D/I_G ratio from 0.1 to 0.8. This suggests that oxidation of graphene occurred.

FIG 24

6. Challenges and Outlook

The previous sections highlight the range and diversity of the current methods within the domain of top-down, liquid-phase exfoliated production. As research surrounding the application of graphene and other 2D materials has developed, two roadmaps have been generated which provide indicative timelines for production advancements [10,13]. Novoselov *et al*. [13] suggested in 2012 that for the following decade, the application of graphene would be driven by progress in production approaches. As evidenced in the current review, both top-down and bottom-up processes have expanded since 2012, but further improvement is necessary. There appears to be a disconnect between the proof-of-concept devices that are constructed on a lab-scale and the more effective approaches emerging as mass-production candidates. Dry mechanical exfoliation, using scotch tape, has been the primary method used at the lab-scale for studying new devices and fundamental physics. While this has resulted in impactful breakthroughs showing graphene's potential, it is a technique which is impractical for large-scale production. As material properties are directly linked to production method, it is likely that this disconnect contributes a certain amount towards the success rate and pace at which graphene-enabled technologies transfer into practical applications.

The scientific and technological objectives set out within the framework of the European Graphene Flagship [10] for large-scale production remain the development of *reliable*, *reproducibl*e, *sustainable* and *safe* approaches that can meet the needs of application areas. These key characteristics have a clear benefit for implementation, however, the previous literature on production approaches are predominantly lacking in these areas.

6.1 Control and characterisation of material properties

There is limited information provided on the statistical methods used, if any, to ensure that the yield, layer distribution, lateral dimensions and defects mentioned are repeatable or a true representation of the production approaches large-scale capability. Material characterisation techniques (AFM, TEM, SEM, etc.) predominantly deal with miniscule sample sizes and so this is challenging. Nonetheless, it is an area that should be addressed to achieve reliable and reproducible outputs. It would also ensure that comparisons between published data for emerging production approaches can be conducted without a concern for underlying measurement bias. This limitation is, however, beginning to receive attention. Recently, Liscio *et al.*[133] presented a thorough statistical analysis on fragmentation and size distributions due to ultrasonic exfoliation. Over 2500 GO sheets were analysed to determine sheet characteristics with confidence. Further effort is needed, both in terms of producing reliable insights on fundamental exfoliation mechanisms, and to develop standard protocols in industry.

The primary focus for the last decade, particularly for top-down production, has been the search for methods which can produce high yield and industrial scale production rates. Properties such as carrier mobility vary by up to six orders of magnitude, depending on the production approach. For the present moment, at least, coverage of a broad set of applications (i.e. from high-frequency transistors to conductive inks) will require a broad range of production approaches. However, in addition to high yield and production rates, demonstrating the ability to tune material properties within individual

approaches would also be beneficial [10]. Research on tuning material properties by varying the operational parameters of a single production approach are currently limited. Paton *et al.* [40] correlated the effect of rotor speed on the resultant mean flake length for a high-shear mixing method. Liu *et al.* [41] used the same exfoliation method, and tested two different rotor sizes, to reveal the variations in flake length and thickness that can occur. Chen *et al.* [107] demonstrated with a spinning disc reactor that both full and partial carbon nanoscrolls can be created, depending on the morphology of the graphite precursor and the varying local microscale fluid mechanics. These liquid-phase exfoliation examples provide evidence that morphological properties of a 2D material can be altered. By refining this ability to construct different material characteristics within a single approach, a broader variety of end-use applications can be targeted.

6.2 Solvents

Liquid-phase exfoliation methods require solvents to assist in production of graphene and form a stable dispersion. Suitable solvents are also required for storing graphene produced via other top-down methods. As it was demonstrated, a good solvent, or a mixture of few solvents, can be selected on the basis of their technical characteristics (see Section 5.2.1) [34]. Ionic surfactants can also be added to poor solvents such as water to effectively assist in exfoliation process and prevent graphene from restacking. Unfortunately, most of the good solvents, surfactants and other relevant chemicals suffer from several issues for any potential scale-up technology as well as post-processing and storage. For instance, the best solvents currently used, e.g. NMP, have a high boiling point making them difficult to separate (and preferably recycle) from the final product without affecting the quality of graphene e.g. oxidation. Moreover, such solvents are toxic and can be incompatible with common materials of construction used in the plant. Thus, when one considers recyclability, health and safety, and environmental aspects of their process, these issues can introduce additional constraints from an engineering and financial perspective.

The unavailability of a suitable solvent that could be used for large-scale production will also cap the throughput per each production line (batch or continuous). From a storage and logistics point of view, it is highly desirable to maximise the concentration of graphene in a solvent and to maintain its initial product specification for as long as possible. A recent study has presented promising results in addressing the aforementioned solvent challenges[134]. Using a selection criteria that matched a range of solvents to a set of ideal dispersion characteristics that include polarity, toxicity, surface tension, viscosity and greenness, Cyrene was discovered to be the most suitable high-performance solvent for sustainable production of graphene. This solvent is environmentally benign, and in this work, facilitated graphene concentrations an order of magnitude greater than NMP.

On the other hand, graphene is a lightweight material and occupies a much smaller volume in solid phase than when dispersed in solvent, resulting in far more economical transportation and storage. So there is also a scope for development of a process that can efficiently separate graphene from its solvent without negatively affecting any of its superior qualities, or encouraging aggregation. Therefore, in order to counteract all of the aforementioned issues, it is probable that there is going to be a need for a synthesis of specific solvents, surfactants or other chemical compounds that possess targeted properties. Furthermore, a unique pathway may also need to be designed that will pre- and post-process graphite/graphene dispersion using an efficient method. It is crucial to design a product which could be effectively utilised by various downstream industries.

6.3 Rheology

The challenges in engineering environmentally-friendly, low boiling point solvents for the dispersion of graphene are non-trivial. High-boiling point solvents, with toxic characteristics, currently produce the highest graphene concentrations. A growing body of empirical and numerical research demonstrate that the long-term stability of monolayer number fraction is limited to tens of days, even for these high performing solvents. Solvent design may be further complicated if the end-use of

liquid-phase exfoliated graphene involves solution processing. In the rapidly emerging area of printable graphene inks for flexible and conductive electronics, rheological properties that include surface tension, viscosity and density impact the printing process [39]. NMP has properties that are suitable for implementation in ink-jet printing, however, both the toxicity and post-treatment requirements (removal at >170ºC) complicate and limit its use. Aqueous surfactant solutions are also limited in practical applications, as the stabilizing agents have an adverse effect on electronic properties. Capasso *et al*. [39] recently tuned the properties of water-ethanol (H_2O/EtOH) mixtures for the exfoliation, dispersion and formulation of graphene-based inks. A 1:1 volume ratio provided a surface tension of 30.9 mN/m, which was within the range required for the ink-jet printing process. The transmittance and conductivity were compared for H_2O/EtOH films and NMP films, both of which had no post-processing applied. A promising outcome was that H_2O/EtOH films could provide higher transmittance at lower electrical resistances by increasing the number of low concentration printing passes. Developing solvents and co-solvent strategies, with tuneable rheology for the end-use, will provide a significant advancement towards introducing this material into practical applications.

6.4 Integration with chemical engineering processes

The growing research field on scale-up of graphene is at a relatively early stage. Most of the previous discussion has surrounded the enhancement of yield, production rate and quality. While this is fundamentally crucial for advancing production methods, there are wider engineering process challenges to be considered. The successful practical implementation of the most promising top-down methods will also rely on seamless system-level integration. Figure 25 provides a summary of the key aspects involved in an end-to-end production process (steps 1 – 6). At present, some components are more developed (e.g. precursor choice, solvent and aqueous surfactant solutions, and exfoliation methods) than others (e.g. high-throughput graphene separation, quality assessment, recycling, storage/handling). This illustration also highlights the dependency of exfoliation methods (step 4) on

factors along the process chain. Robust technologies, capable of easily integrating within this process chain, have a distinct advantage. A holistic view of the entire chemical engineering process, therefore, is required for graphene production to translate from the laboratory to industrial scales.

FIG 25

6.5 Modelling and simulation

The liquid-phase exfoliation process is complex, covering a range of length scales that span 6-9 orders of magnitude, from the device level (10^{-3}-10^{0} metres) to the graphene end-product (nanometres). Processing time is typically over hours, whereas the individual exfoliation mechanisms can occur at fractions of a microsecond. Examples of this are in the approaches that utilize the rapid bubble collapse during cavitation [135] to induce exfoliation of graphite. In addition to a discrete phase (graphite), multiple continuous phases (liquid and gas) exist in shear-driven methods such as sonication, jet cavitation, and thin film approaches like the spinning disc and vortex fluidic devices. Multiple species (intercalants, oxidising agents) exist in chemical and electrochemical methods, and the microwave exfoliation method (Section 5.4.2) is an example of a multi-physics phenomenon. The breadth of transport phenomena and scales is, therefore, significant. This makes it challenging to analyse the exfoliation processes in high fidelity through experiments alone.

Numerical modelling is a powerful tool for providing fundamental insights that can be validated with experiments. Molecular dynamics has already been used to understand the interactions between graphene sheets, when dispersed in various solvents [66] and aqueous surfactant solutions [71] (see Section 5.2). Chen *et al.*[107] observed carbon nanoscrolls in exfoliation experiments, and utilised molecular dynamics to study the conditions that favour such scrolling behaviour. Other techniques, such as computational fluid dynamics (CFD), can elucidate fluid and transport phenomena at larger scales where a continuum representation is valid. These modelling and simulation tools are well-established in chemical engineering disciplines, but have yet to be utilised to their full potential for liquid-phase

exfoliation. As this research field continues to develop, it is anticipated that these tools will also be important in practice, for the prediction and optimisation of production performance.

6.6 Other 2D materials

In addition to the improvements necessary for graphene production, other 2D material research has opened exciting new avenues for large-scale production. Similar to graphite, transition metal dichalcogenides (TMDs) and transition metal oxides (TMOs) also have a layered structure with van der Waals forces holding individual layers together. There is potential to discover many other layered materials with novel properties that have yet to be isolated into 2D form. These materials can be realized over the next 5 years on a large-scale by extending proven production technologies for graphene to other 2D crystals. An example of this is the recent work by Cullen *et al.*[136] on dissolution of numerous 2D materials (Graphene, TiS_2, $MoSe_2$, Bi_2Te_3) to form ionic liquids.

Long-term research challenges beyond the next decade include the production of 2D heterostructures, or stacked layers of different materials which are held together through van der Waals forces. These materials have shown uniquely beneficial properties at the lab-scale, such as the highest-mobility graphene transistors, created by encapsulating graphene with h-BN using CVD [137]. Flexible photovoltaics have also been demonstrated utilizing optically active semiconducting layers (TMDs) with graphene as transparent electrodes [138]. Novosolev *et al.* [139] noted that this topic is now at a stage where graphene was 10 years ago, with *"plenty of interesting science and unclear prospects for mass-production"*. If research efforts grow at a similar rate to what has been realized for graphene over the past decade, there is an exciting future for both the scientific and application areas of 2D material production.

7. Conclusions

The topic of large-scale production has grown considerably over the last decade to establish itself as a scientific field within the overall graphene research domain. Developments have evolved into

process routes that can now be categorized under two independent production approaches. These approaches, defined as ‘top-down’ and ‘bottom-up’, produce a variety of graphene-based materials, including monolayer and multi-layer sheets, nanoscrolls and graphene oxides. Liquid-phase exfoliation is a top-down method which has a high potential for scale-up. This approach has demonstrated the highest production rates (~ 6 g h^{-1}), but with comparatively low yield (< 5%). Electrochemical exfoliation achieved high yield graphene oxides in studies using HOPG (> 70%), and when combined with shear-assisted flows this method has produced low-defect flakes, which have some of the largest dimensions (~10 µm) for top-down approaches.

The notable disparity in product characteristics across top-down approaches is linked to the multiple exfoliation mechanisms that have been investigated. Shear, collision, cavitation, chemical and electrochemical intercalation, the type of graphite precursor, solvent selection, and the inclusion of post-processing techniques such as centrifugation all impact graphene output. In contrast, bottom-up methods such as CVD and epitaxial growth, are less diverse and have the capability to synthesize high-quality monolayer sheets with larger lateral sizes ranging from tens of μm^2 to several cm^2. While this is preferable for applications that require high carrier mobility (~ 10^5 cm^2 V^{-1} s^{-1}), there is no clear indication of potential rates of production. Bottom-up methods can also require post-processing steps to remove the graphene sheets from the substrate on which it has been grown. The lack of convergence towards a single all-encompassing method is due to the material requirements of the potential end-use applications. Energy storage and generation, flexible and printed electronics, and composites can be addressed using top-down approaches. High-end electronics and the ability to integrate with semiconductor devices are applications which need a high-quality product achievable by bottom-up approaches.

Across all production approaches, it is anticipated that the future developments for graphene will be around tunable morphology, proven reliability and repeatability, and sustainable and safe

implementation in chemical engineering processes. This will ensure that scientific outputs can be translated into commercial technologies that can meet application demand. Finally, a summary comparing the production characteristics of different methods can be seen in Table 4.

Table 4: Summary of the bottom-up and top-down production methods, highlighting key graphene characteristics as well as the advantages and disadvantages of the various approaches.

Method	Advantages	Disadvantages	Process details	Raman D/G*	Selectivity	Yield (wt%)	Production rate (g/h)**	Reference
Chemical Vapor Deposition (CVD)	Potentially high production rate	Defective graphene Harsh conditions	From sodium ethoxide	1 (532 nm)	Higher selectivity to 4 layers	-	-	[140]
			Atmospheric Pressure CVD	-	-	-	-	[141]
			Cold-wall CVD	0.2				[142]
			High speed roll to roll	0.16	-	-	-	[143]
Arc Discharge	High quantity of graphene can be produced Low processing time required	Defective graphene	In Hydrogen	-	2-4 layers	10-20	-	[144]
			In N_2 and H_2 with AC current	0.55-0.92 (633nm)	Mainly 2 layers	5.3	25.2	[28]
			Helium with O_2 and H_2	~0.8 (514.5nm)	6 layers	-	-	[145]
			H_2-inert gas mixture	0.26-0.31	Mostly 2-4 layers with a small portion of 5-10 layers	-	~3	[146]
Epitaxial growth	High coverage of monolayer across the metal surface	Defective graphene	On SiC	-	1-2 layers	-	-	[147]
Sonication	Low cost	Defective graphene Low concentration of graphene	In pyrene surfactant	0.33 (633nm)		-	0.02	[74]
			In NMP	Very low D band observed	~28% monolayer. <5 layers	8.3-12	8×10^{-3}	[18]
			In surfactant	0.93 (514nm)	-	-	0.018	[148]
			In isopropanol	0.2-0.4 (633nm)	-	-	0.015	[149]
			In NMP	0.15 (514nm)	-	-	-	[150]
			In chloroform	-	-	-	8×10^{-3}	[151]
			In surfactant, NMP and *ortho*-dichlorobenzene (o-DCM)	-	~28% monolayer, 19% bilayer.	1.2	-	[152]
			In gum Arabic	0.25 (633nm)	Mainly 5-10 layers	5	5×10^{-3}	[153]
			In non-ionic polymeric surfactant	0.35	Mainly 2-3 layers	-	-	[154]
			In surfactants	-	Mainly 4 layers	0.5	5×10^{-3}	[27]
			In NMP	0.2-0.5	90% less than 5 layers	4	$\sim5\times10^{-3}$	[20]

			In SDBS surfactant	0.4	3% monolayer, 40% <5layers	3	-	[44]
			Two-step in NMP	<0.5 (633nm)	3-4 layers	19	7.5×10^{-3}	[21]
Solvothermal	Selective to monolayer graphene	Long processing time Harsh conditions	In forming gas	-	1-2 layers	10-12	8.3×10^{-5}	[26]
			In tartaric acid	0.06	~95% monolayer	-	-	[94]
Supercritical Fluid	High yield	High pressure	In sulphate dispersant	-	10 layers	40	0.8	[47]
			In NMP, DMF	-	3-10 layers mostly	10	3.3×10^{-4}	[102]
			Shear assisted	0.56	~70% 5-8 layers	90	0.9	[43]
			Ultra-sonication assisted	-	24% 1 layer, 44% 2 layers, 26% tri layers	21.5	0.11	[17]
Microwave	High yield Short processing time Simple and implemented easily technology	Difficult solvent/graphene separation	In Ionic liquid	0.14	95% monolayer	93	0.02	[24]
Vortex fluidic	Simple set-up with minimal issues during the operation	Very low yield	In NMP	-	-	1	-	[104]
Taylor-Couette	High quality graphene	Low yield	In NMP	0.14	90% less than 5 layers	5	-	[106]
Pressure Driven	Simple process High quality graphene	Low yield	Jet Cavitation	0.38	70% less than 5 layers	5	0.25	[23]
High shear mixing	High production rate High quality graphene	Precise control of operating conditions required Defective graphene	In IPA-water	0.14.0.18 (514nm)	Mainly less than 4 layers	8	-	[41]
			Mixer	0.17-0.37	5-8 layers	-	5.3	[40]
			Kitchen blender	0.12	-	7.3	9.2×10^{-3}	[109]
Micromechanical cleavage	High quality graphene Selective to monolayer	Expensive Long processing time	With scotch tape	-	monolayer	-	-	2
			With wedge	0.86	-	50	-	[155]
			With three roll mill	0.06	50% monolayer	90	Max- 0.075	[16]
Ball milling	Cost effective	Very long processing time	In SDS	0.6-0.7 (532nm)		50-75	1.5-2.5	[22]
			In DMF	0.34	1-3 layers	-	-	[156]

	Potential for graphene functionalization	Defective graphene	In methanol and 1-pyrene carboxylic acid	0.24-0.38 (488nm)	5-10 layers	-	-	[157]
			In sulphur	-	95% <10 layers	-	-	[158]
			In gases	1.32	25% monolayer. Most less than 5 layers	-	-	[159]
Spinning disc	Possible continuous flow configuration	Long recycling time	In NMP	-	-	1	-	[107]
Chemical exfoliation	Cost effective	Low production rate Defective graphene	By acetic acid	1.1	-	-	0.06	[160]
			By Na in NH_3	1.4	-		0.33	[161]
			Staudenmaier	-	-	-	1×10-3	[162]
			Hummer method	-		-	0.45	[163]
Electrochemical exfoliation	High yield	Expensive Defective graphene Limited number of studies reported	Anodic exfoliation	0.25	85% less than 3 layer. 72% 1-2 layers	75	32.6	[25]
			Anodic with Poly(sodium-4-styrenesulfonate) PSS	-	2-5 layers	15	-	[50]
			Anodic with copper acid	0.92	1-6 layers	-	-	[125]
			Anodic with sulfonic acid	0.32	5% 1-2 layers 78% 4 layers	-	-	[126]
			Cathodic with LiOH	0.29	2-4 layers	80	1.1	[19]
			Cathodic with Li^+	1.1	-	40	-	[132]
			Cathodic with DMSO	0.5	5% monolayer	-	-	[122]
			Cathodic with ionic liquids	0.05	2-5 layers	25	5.56×10-3	[29]
			Anodic with shear assisted	0.1	75% less than 4 layers	-	-	[54]
Chaotic flow with sonication	Short processing time	Low yield	In NMP	-	Less than 3 layers	7.2	-	[42]

* The wavelength in parenthesis indicates the wavelength of the laser used for Raman spectroscopy analyses.

**Production rate was estimated from best possible yield (mass of graphene / the mass of the initial graphite precursor) and processing times from the paper

8. Acknowledgement

JS and OKM would like to thank the European Commission for their financial support. This project has received funding from the European Union's Horizon 2020 research and innovation programme under the Marie Skłodowska-Curie grant agreement No 707340.

9. List of abbreviations

Abbreviation	Definition
2D	two-dimensional
3D	three-dimensional
1D	one-dimensional
0D	zero-dimensional
BNNS	boron nitride nanosheets
TMDs	transition metal dichalcogenides
TMOs	transition metal oxides
TEM	transmission electron microscopy
MLG	multi-layer graphene (also known as few-layer)
N_l	layer numbers
GO	graphene oxide
rGO	reduced graphene oxide
SEM	scanning electron microscopy
HRTEM	high resolution transmission electron microscopy
AFM	atomic force microscopy
SWCNT	single-walled carbon nanotube
I_{2D}	Raman 2D peak
I_D	Raman D peak

I_G	Raman G peak
XPS	X-ray photoelectron spectroscopy
SAED	selected area electron diffraction
h-BN	hexagonal boron nitride
$\dot{\gamma}$	shear rate
CPO	cyclopentanone
_	Flory-Huggins parameter
MD	Molecular dynamics
PMF	the potential of mean force
SDBS	Sodium dodecylbenzene sulfonate
SC	sodium cholate
GIC	graphite intercalated compound
PGO	pristine graphite oxide
_	liquid density
_	liquid viscosity
GS	graphene sheet
C_G	concentration of graphene (supernatant)
HOPG	Highly Oriented Pyrolytic Graphite
IP	intellectual property

10. References

1. Paulus GL, Shimizu S, Abrahamson JT, Zhang J, Hilmer AJ, Strano MS. The chemical engineering of low-dimensional materials. *Aiche Journal*. 2011;57(5):1104-1118.

2. Novoselov KS, Geim AK, Morozov SV, et al. Electric field effect in atomically thin carbon films. *Science.* 2004;306(5696):666-669.
3. Mayorov AS, Gorbachev RV, Morozov SV, et al. Micrometer-scale ballistic transport in encapsulated graphene at room temperature. *Nano letters.* 2011;11(6):2396-2399.
4. Balandin AA, Ghosh S, Bao W, et al. Superior thermal conductivity of single-layer graphene. *Nano letters.* 2008;8(3):902-907.
5. Lee C, Wei X, Kysar JW, Hone J. Measurement of the elastic properties and intrinsic strength of monolayer graphene. *science.* 2008;321(5887):385-388.
6. Nair RR, Blake P, Grigorenko AN, et al. Fine structure constant defines visual transparency of graphene. *Science.* 2008;320(5881):1308-1308.
7. Bunch JS, Verbridge SS, Alden JS, et al. Impermeable atomic membranes from graphene sheets. *Nano letters.* 2008;8(8):2458-2462.
8. Desai SB, Madhvapathy SR, Sachid AB, et al. MoS2 transistors with 1-nanometer gate lengths. *Science.* 2016;354(6308):99-102.
9. Lei W, Portehault D, Liu D, Qin S, Chen Y. Porous boron nitride nanosheets for effective water cleaning. *Nature communications.* 2013;4:1777.
10. Ferrari AC, Bonaccorso F, Fal'Ko V, et al. Science and technology roadmap for graphene, related two-dimensional crystals, and hybrid systems. *Nanoscale.* 2015;7(11):4598-4810.
11. Wei Y, Sun Z. Liquid-phase exfoliation of graphite for mass production of pristine few-layer graphene. *Current Opinion in Colloid & Interface Science.* 2015;20(5–6):311-321.
12. Blake P, Brimicombe PD, Nair RR, et al. Graphene-based liquid crystal device. *Nano letters.* 2008;8(6):1704-1708.
13. Novoselov KS, Fal V, Colombo L, Gellert P, Schwab M, Kim K. A roadmap for graphene. *Nature.* 2012;490(7419):192-200.

14. Graphene-info. “Future Markets predicts graphene to reach $250 million at component and material levels in 2017”. http://www.graphene-info.com/future-markets-predicts-graphene-reach-250-million-component-and-material-levels-2017. Accessed Jan 31, 2017.

15. León V, Rodriguez AM, Prieto P, Prato M, Vázquez E. Exfoliation of graphite with triazine derivatives under ball-milling conditions: preparation of few-layer graphene via selective noncovalent interactions. *ACS nano.* 2014;8(1):563-571.

16. Chen J, Duan M, Chen G. Continuous mechanical exfoliation of graphene sheets via three-roll mill. *Journal of Materials Chemistry.* 2012;22(37):19625-19628.

17. Gao Y, Shi W, Wang W, et al. Ultrasonic-assisted production of graphene with high yield in supercritical CO2 and its high electrical conductivity film. *Industrial & Engineering Chemistry Research.* 2014;53(7):2839-2845.

18. Hernandez Y, Nicolosi V, Lotya M, et al. High-yield production of graphene by liquid-phase exfoliation of graphite. *Nature nanotechnology.* 2008;3(9):563-568.

19. Huang H, Xia Y, Tao X, et al. Highly efficient electrolytic exfoliation of graphite into graphene sheets based on Li ions intercalation–expansion–microexplosion mechanism. *Journal of Materials Chemistry.* 2012;22(21):10452-10456.

20. Khan U, O'Neill A, Lotya M, De S, Coleman JN. High-Concentration Solvent Exfoliation of Graphene. *Small.* 2010;6(7):864-871.

21. Khan U, Porwal H, O’Neill A, Nawaz K, May P, Coleman JN. Solvent-exfoliated graphene at extremely high concentration. *Langmuir.* 2011;27(15):9077-9082.

22. Knieke C, Berger A, Voigt M, Taylor RNK, Röhrl J, Peukert W. Scalable production of graphene sheets by mechanical delamination. *Carbon.* 2010;48(11):3196-3204.

23. Liang S, Yi M, Shen Z, Liu L, Zhang X, Ma S. One-step green synthesis of graphene nanomesh by fluid-based method. *RSC Advances.* 2014;4(31):16127-16131.

24. Matsumoto M, Saito Y, Park C, Fukushima T, Aida T. Ultrahigh-throughput exfoliation of graphite into pristine ‘single-layer’graphene using microwaves and molecularly engineered ionic liquids. *Nature chemistry*. 2015;7(9):730-736.

25. Parvez K, Wu Z-S, Li R, et al. Exfoliation of graphite into graphene in aqueous solutions of inorganic salts. *Journal of the American Chemical Society*. 2014;136(16):6083-6091.

26. Qian W, Hao R, Hou Y, et al. Solvothermal-assisted exfoliation process to produce graphene with high yield and high quality. *Nano Research.* 2009;2(9):706-712.

27. Smith RJ, Lotya M, Coleman JN. The importance of repulsive potential barriers for the dispersion of graphene using surfactants. *New Journal of Physics.* 2010;12(12):125008.

28. Wu X, Liu Y, Yang H, Shi Z. Large-scale synthesis of high-quality graphene sheets by an improved alternating current arc-discharge method. *RSC Advances.* 2016;6(95):93119-93124.

29. Yang Y, Lu F, Zhou Z, Song W, Chen Q, Ji X. Electrochemically cathodic exfoliation of graphene sheets in room temperature ionic liquids N-butyl, methylpyrrolidinium bis (trifluoromethylsulfonyl) imide and their electrochemical properties. *Electrochimica Acta.* 2013;113:9-16.

30. Terrones M, Botello-Méndez AR, Campos-Delgado J, et al. Graphene and graphite nanoribbons: Morphology, properties, synthesis, defects and applications. *Nano Today.* 2010;5(4):351-372.

31. Wissler M. Graphite and carbon powders for electrochemical applications. *Journal of Power Sources.* 2006;156(2):142-150.

32. Wu Z-S, Ren W, Gao L, Liu B, Jiang C, Cheng H-M. Synthesis of high-quality graphene with a pre-determined number of layers. *Carbon.* 2009;47(2):493-499.

33. Knirsch KC, Englert JM, Dotzer C, Hauke F, Hirsch A. Screening of the chemical reactivity of three different graphite sources using the formation of reductively alkylated graphene as a model reaction. *Chemical Communications.* 2013;49(92):10811-10813.

34. Arao Y, Mori F, Kubouchi M. Efficient solvent systems for improving production of few-layer graphene in liquid phase exfoliation. *Carbon.* 2017;118:18-24.

35. Kozhemyakina NV, Eigler S, Dinnebier RE, Inayat A, Schwieger W, Hirsch A. Effect of the structure and morphology of natural, synthetic and post-processed graphites on their dispersibility and electronic properties. *Fullerenes, Nanotubes and Carbon Nanostructures.* 2013;21(9):804-823.

36. Warner JH, Schäffel F, Bachmatiuk A, Rümmeli MH. Chapter 4 - Methods for Obtaining Graphene. *Graphene*: Elsevier; 2013:129-228.

37. Çelik Y, Flahaut E, Suvacı E. A comparative study on few-layer graphene production by exfoliation of different starting materials in a low boiling point solvent. *FlatChem.* 2017;1:74-88.

38. Liu L, Qing M, Wang Y, Chen S. Defects in graphene: generation, healing, and their effects on the properties of graphene: a review. *Journal of Materials Science & Technology.* 2015;31(6):599-606.

39. Capasso A, Castillo ADR, Sun H, Ansaldo A, Pellegrini V, Bonaccorso F. Ink-jet printing of graphene for flexible electronics: an environmentally-friendly approach. *Solid State Communications.* 2015;224:53-63.

40. Paton KR, Varrla E, Backes C, et al. Scalable production of large quantities of defect-free few-layer graphene by shear exfoliation in liquids. *Nature materials.* 2014;13(6):624-630.

41. Liu L, Shen Z, Yi M, Zhang X, Ma S. A green, rapid and size-controlled production of high-quality graphene sheets by hydrodynamic forces. *RSC Advances.* 2014;4(69):36464-36470.

42. Liu W, Tanna VA, Yavitt BM, Dimitrakopoulos C, Winter HH. Fast Production of High-Quality Graphene via Sequential Liquid Exfoliation. *ACS applied materials & interfaces.* 2015;7(49):27027-27030.

43. Li L, Xu J, Li G, et al. Preparation of graphene nanosheets by shear-assisted supercritical CO 2 exfoliation. *Chemical Engineering Journal.* 2016;284:78-84.

44. Lotya M, Hernandez Y, King PJ, et al. Liquid phase production of graphene by exfoliation of graphite in surfactant/water solutions. *Journal of the American Chemical Society*. 2009;131(10):3611-3620.

45. Guardia L, Fernández-Merino M, Paredes J, et al. High-throughput production of pristine graphene in an aqueous dispersion assisted by non-ionic surfactants. *Carbon*. 2011;49(5):1653-1662.

46. Liu Y, Yuan G, Jiang Z, Yao Z, Yue M. Solvothermal synthesis of graphene nanosheets as the electrode materials for supercapacitors. *Ionics*. 2015;21(3):801-808.

47. Pu N-W, Wang C-A, Sung Y, Liu Y-M, Ger M-D. Production of few-layer graphene by supercritical CO 2 exfoliation of graphite. *Materials Letters*. 2009;63(23):1987-1989.

48. Chen W, Yan L, Bangal PR. Preparation of graphene by the rapid and mild thermal reduction of graphene oxide induced by microwaves. *Carbon*. 2010;48(4):1146-1152.

49. Yi M, Shen Z, Ma S, Zhang X. A mixed-solvent strategy for facile and green preparation of graphene by liquid-phase exfoliation of graphite. *Journal of Nanoparticle Research*. 2012;14(8):1003.

50. Wang G, Wang B, Park J, Wang Y, Sun B, Yao J. Highly efficient and large-scale synthesis of graphene by electrolytic exfoliation. *Carbon*. 2009;47(14):3242-3246.

51. Tran TS, Park SJ, Yoo SS, Lee T-R, Kim T. High shear-induced exfoliation of graphite into high quality graphene by Taylor–Couette flow. *RSC Advances*. 2016;6(15):12003-12008.

52. Zhang M, Parajuli RR, Mastrogiovanni D, et al. Production of graphene sheets by direct dispersion with aromatic healing agents. *Small*. 2010;6(10):1100-1107.

53. Cooper AJ, Wilson NR, Kinloch IA, Dryfe RA. Single stage electrochemical exfoliation method for the production of few-layer graphene via intercalation of tetraalkylammonium cations. *Carbon*. 2014;66:340-350.

54. Shinde DB, Brenker J, Easton CD, Tabor RF, Neild A, Majumder M. Shear assisted electrochemical exfoliation of graphite to graphene. *Langmuir*. 2016;32(14):3552-3559.

55. Liu J, Notarianni M, Will G, Tiong VT, Wang H, Motta N. Electrochemically exfoliated graphene for electrode films: effect of graphene flake thickness on the sheet resistance and capacitive properties. *Langmuir*. 2013;29(43):13307-13314.

56. Vadukumpully S, Paul J, Valiyaveettil S. Cationic surfactant mediated exfoliation of graphite into graphene flakes. *Carbon.* 2009;47(14):3288-3294.

57. Bergin SD, Nicolosi V, Streich PV, et al. Towards Solutions of Single-Walled Carbon Nanotubes in Common Solvents. *Advanced Materials.* 2008;20(10):1876-1881.

58. Ausman KD, Piner R, Lourie O, Ruoff RS, Korobov M. Organic solvent dispersions of single-walled carbon nanotubes: toward solutions of pristine nanotubes. *The Journal of Physical Chemistry B.* 2000;104(38):8911-8915.

59. Furtado C, Kim U, Gutierrez H, Pan L, Dickey E, Eklund PC. Debundling and dissolution of single-walled carbon nanotubes in amide solvents. *Journal of the American Chemical Society*. 2004;126(19):6095-6105.

60. Ham HT, Choi YS, Chung IJ. An explanation of dispersion states of single-walled carbon nanotubes in solvents and aqueous surfactant solutions using solubility parameters. *Journal of Colloid and Interface Science*. 2005;286(1):216-223.

61. Detriche S, Zorzini G, Colomer J-F, Fonseca A, Nagy J. Application of the Hansen solubility parameters theory to carbon nanotubes. *Journal of nanoscience and nanotechnology*. 2008;8(11):6082-6092.

62. Hernandez Y, Lotya M, Rickard D, Bergin SD, Coleman JN. Measurement of multicomponent solubility parameters for graphene facilitates solvent discovery. *Langmuir*. 2009;26(5):3208-3213.

63. Coleman JN. Liquid exfoliation of defect-free graphene. *Accounts of chemical research.* 2012;46(1):14-22.

64. Bergin SD, Sun Z, Rickard D, Streich PV, Hamilton JP, Coleman JN. Multicomponent solubility parameters for single-walled carbon nanotube− solvent mixtures. *ACS nano.* 2009;3(8):2340-2350.

65. Hansen CM. *Hansen solubility parameters: a user's handbook.* CRC press; 2007.

66. Shih C-J, Lin S, Strano MS, Blankschtein D. Understanding the stabilization of liquid-phase-exfoliated graphene in polar solvents: molecular dynamics simulations and kinetic theory of colloid aggregation. *Journal of the American Chemical Society.* 2010;132(41):14638-14648.

67. Israelachvili JN. *Intermolecular and surface forces.* Academic press; 2015.

68. Geng H-Z, Lee DS, Kim KK, Han GH, Park HK, Lee YH. Absorption spectroscopy of surfactant-dispersed carbon nanotube film: modulation of electronic structures. *Chemical Physics Letters.* 2008;455(4):275-278.

69. Vigolo B, Penicaud A, Coulon C, et al. Macroscopic fibers and ribbons of oriented carbon nanotubes. *Science.* 2000;290(5495):1331-1334.

70. Wenseleers W, Vlasov II, Goovaerts E, Obraztsova ED, Lobach AS, Bouwen A. Efficient Isolation and Solubilization of Pristine Single-Walled Nanotubes in Bile Salt Micelles. *Advanced Functional Materials.* 2004;14(11):1105-1112.

71. Lin S, Shih C-J, Strano MS, Blankschtein D. Molecular insights into the surface morphology, layering structure, and aggregation kinetics of surfactant-stabilized graphene dispersions. *Journal of the American Chemical Society.* 2011;133(32):12810-12823.

72. Coleman JN. Liquid-Phase Exfoliation of Nanotubes and Graphene. *Advanced Functional Materials.* 2009;19(23):3680-3695.

73. Lotya M, King PJ, Khan U, De S, Coleman JN. High-concentration, surfactant-stabilized graphene dispersions. *ACS nano.* 2010;4(6):3155-3162.

74. Parviz D, Das S, Ahmed HT, Irin F, Bhattacharia S, Green MJ. Dispersions of non-covalently functionalized graphene with minimal stabilizer. *Acs Nano.* 2012;6(10):8857-8867.

75. Sun Z, Masa J, Liu Z, Schuhmann W, Muhler M. Highly concentrated aqueous dispersions of graphene exfoliated by sodium taurodeoxycholate: dispersion behavior and potential application as a catalyst support for the oxygen-reduction reaction. *Chemistry-A European Journal*. 2012;18(22):6972-6978.

76. Ayán-Varela M, Paredes J, Guardia L, et al. Achieving extremely concentrated aqueous dispersions of graphene flakes and catalytically efficient graphene-metal nanoparticle hybrids with flavin mononucleotide as a high-performance stabilizer. *ACS applied materials & interfaces*. 2015;7(19):10293-10307.

77. Paredes J, Villar-Rodil S. Biomolecule-assisted exfoliation and dispersion of graphene and other two-dimensional materials: a review of recent progress and applications. *Nanoscale*. 2016;8(34):15389-15413.

78. Marcaccio M, Paolucci F. *Making and exploiting fullerenes, graphene, and carbon nanotubes*. Springer; 2014.

79. Fogden S, Howard CA, Heenan RK, Skipper NT, Shaffer MS. Scalable method for the reductive dissolution, purification, and separation of single-walled carbon nanotubes. *ACS nano*. 2011;6(1):54-62.

80. Pénicaud A, Drummond C. Deconstructing graphite: Graphenide solutions. *Accounts of chemical research*. 2012;46(1):129-137.

81. Allemand P, Srdanov G, Koch A, et al. The unusual electron spin resonance of fullerene C60 anion radical. *Journal of the American Chemical Society*. 1991;113(7):2780-2781.

82. Catheline A, Ortolani L, Morandi V, et al. Solutions of fully exfoliated individual graphene flakes in low boiling point solvents. *Soft Matter*. 2012;8(30):7882-7887.

83. Bepete G, Anglaret E, Ortolani L, et al. Surfactant-free single-layer graphene in water. *Nature Chemistry*. 2016.

84. Yi M, Shen Z. A review on mechanical exfoliation for the scalable production of graphene. *Journal of Materials Chemistry A*. 2015;3(22):11700-11715.

85. Chen J, Li Y, Huang L, Li C, Shi G. High-yield preparation of graphene oxide from small graphite flakes via an improved Hummers method with a simple purification process. *Carbon.* 2015;81:826-834.

86. He D, Shen L, Zhang X, Wang Y, Bao N, Kung HH. An efficient and eco-friendly solution-chemical route for preparation of ultrastable reduced graphene oxide suspensions. *AIChE Journal.* 2014;60(8):2757-2764.

87. Eigler S, Dotzer C, Hirsch A. Visualization of defect densities in reduced graphene oxide. *Carbon.* 2012;50(10):3666-3673.

88. Rozada R, Paredes JI, López MJ, et al. From graphene oxide to pristine graphene: revealing the inner workings of the full structural restoration. *Nanoscale.* 2015;7(6):2374-2390.

89. Park S, Ruoff RS. Chemical methods for the production of graphenes. *Nature nanotechnology.* 2009;4(4):217.

90. Gengler RY, Spyrou K, Rudolf P. A roadmap to high quality chemically prepared graphene. *Journal of Physics D: Applied Physics.* 2010;43(37):374015.

91. Thakur S, Karak N. Alternative methods and nature-based reagents for the reduction of graphene oxide: A review. *Carbon.* 2015;94(Supplement C):224-242.

92. Parvez K, Yang S, Feng X, Müllen K. Exfoliation of graphene via wet chemical routes. *Synthetic Metals.* 2015;210:123-132.

93. Yu P, Lowe SE, Simon GP, Zhong YL. Electrochemical exfoliation of graphite and production of functional graphene. *Current Opinion in Colloid & Interface Science.* 2015;20(5):329-338.

94. Al-Hazmi FS, Al-Harbi GH, Beall GW, Al-Ghamdi A, Obaid A, Mahmoud WE. Synthesis and structure of high quality graphene prepared via solvothermal exfoliation of intercalated graphite flakes. *Superlattices and Microstructures.* 2015;86:270-274.

95. Sasikala SP, Poulin P, Aymonier C. Advances in Subcritical Hydro-/Solvothermal Processing of Graphene Materials. *Advanced Materials.* 2017.

96. Liu X, Liu J, Zhan D, et al. Repeated microwave-assisted exfoliation of expandable graphite for the preparation of large scale and high quality multi-layer graphene. *RSC Advances.* 2013;3(29):11601-11606.

97. Sridhar V, Jeon J-H, Oh I-K. Synthesis of graphene nano-sheets using eco-friendly chemicals and microwave radiation. *Carbon.* 2010;48(10):2953-2957.

98. Liu X, Zhan D, Chao D, et al. Microwave-assisted production of giant graphene sheets for high performance energy storage applications. *Journal of Materials Chemistry A.* 2014;2(31):12166-12170.

99. Hummers Jr WS, Offeman RE. Preparation of graphitic oxide. *Journal of the American Chemical Society.* 1958;80(6):1339-1339.

100. Lin J, Huang Y, Wang S, Chen G. Microwave-assisted rapid exfoliation of graphite into graphene by using ammonium bicarbonate as the intercalation agent. *Industrial & Engineering Chemistry Research.* 2017;56(33):9341-9346.

101. Tang Y, Lee CS, Chen Z, et al. High-quality graphenes via a facile quenching method for field-effect transistors. *Nano letters.* 2009;9(4):1374-1377.

102. Rangappa D, Sone K, Wang M, et al. Rapid and Direct Conversion of Graphite Crystals into High-Yielding, Good-Quality Graphene by Supercritical Fluid Exfoliation. *Chemistry–A European Journal.* 2010;16(22):6488-6494.

103. Song N, Jia J, Wang W, Gao Y, Zhao Y, Chen Y. Green production of pristine graphene using fluid dynamic force in supercritical CO2. *Chemical Engineering Journal.* 2016;298:198-205.

104. Chen X, Dobson JF, Raston CL. Vortex fluidic exfoliation of graphite and boron nitride. *Chemical Communications.* 2012;48(31):3703-3705.

105. Wahid MH, Eroglu E, Chen X, Smith SM, Raston CL. Functional multi-layer graphene–algae hybrid material formed using vortex fluidics. *Green Chemistry.* 2013;15(3):650-655.

106. Tran TS, Park SJ, Yoo SS, Lee T-R, Kim T. High shear-induced exfoliation of graphite into high quality graphene by Taylor–Couette flow. *RSC Adv.* 2016;6(15):12003-12008.

107. Chen X, Boulos RA, Dobson JF, Raston CL. Shear induced formation of carbon and boron nitride nano-scrolls. *Nanoscale.* 2013;5(2):498-502.

108. Yi M, Shen Z. Kitchen blender for producing high-quality few-layer graphene. *Carbon.* 2014;78:622-626.

109. Varrla E, Paton KR, Backes C, et al. Turbulence-assisted shear exfoliation of graphene using household detergent and a kitchen blender. *Nanoscale.* 2014;6(20):11810-11819.

110. Ashokkumar M, Mason TJ. Sonochemistry. *Kirk-Othmer Encyclopedia of Chemical Technology.* 2007.

111. Alzari V, Nuvoli D, Sanna R, et al. In situ production of high filler content graphene-based polymer nanocomposites by reactive processing. *Journal of Materials Chemistry.* 2011;21(41):16544-16549.

112. Bourlinos AB, Georgakilas V, Zboril R, Steriotis TA, Stubos AK. Liquid-phase exfoliation of graphite towards solubilized graphenes. *Small.* 2009;5(16):1841-1845.

113. Sim Y, Park J, Kim YJ, Seong M-J, Hong S. Synthesis of graphene layers using graphite dispersion in aqueous surfactant solutions. *J Korean Phys Soc.* 2011;58(4):938-942.

114. Yi M, Shen Z, Zhang X, Ma S. Achieving concentrated graphene dispersions in water/acetone mixtures by the strategy of tailoring Hansen solubility parameters. *Journal of Physics D: Applied Physics.* 2012;46(2):025301.

115. Zhou X, Wu T, Ding K, Hu B, Hou M, Han B. Dispersion of graphene sheets in ionic liquid [bmim][PF6] stabilized by an ionic liquid polymer. *Chem. Commun.* 2010;46(3):386-388.

116. Lavin-Lopez M, Valverde JL, Sanchez-Silva L, Romero A. Solvent-Based Exfoliation via Sonication of Graphitic Materials for Graphene Manufacture. *Industrial & Engineering Chemistry Research.* 2016;55(4):845-855.

117. Ciesielski A, Samorì P. Graphene via sonication assisted liquid-phase exfoliation. *Chemical Society Reviews.* 2014;43(1):381-398.

118. Muthoosamy K, Manickam S. State of the art and recent advances in the ultrasound-assisted synthesis, exfoliation and functionalization of graphene derivatives. *Ultrasonics Sonochemistry*. 2017;39(Supplement C):478-493.

119. Liu L, Shen Z, Liang S, Yi M, Zhang X, Ma S. Graphene for reducing bubble defects and enhancing mechanical properties of graphene/cellulose acetate composite films. *Journal of Materials Science*. 2014;49(1):321-328.

120. Liang S, Shen Z, Yi M, et al. Effects of Processing Parameters on Massive Production of Graphene by Jet Cavitation. *Journal of nanoscience and nanotechnology*. 2015;15(4):2686-2694.

121. Liu J, Yang H, Zhen SG, et al. A green approach to the synthesis of high-quality graphene oxide flakes via electrochemical exfoliation of pencil core. *RSC Advances*. 2013;3(29):11745-11750.

122. Abdelkader AM, Kinloch IA, Dryfe RA. Continuous electrochemical exfoliation of micrometer-sized graphene using synergistic ion intercalations and organic solvents. *ACS applied materials & interfaces*. 2014;6(3):1632-1639.

123. Abdelkader A, Cooper A, Dryfe R, Kinloch I. How to get between the sheets: a review of recent works on the electrochemical exfoliation of graphene materials from bulk graphite. *Nanoscale*. 2015;7(16):6944-6956.

124. Li P, Bae SH, Zan QY, Kim NH, Lee JH. One-step process for the exfoliation and surface modification of graphene by electrochemical method. Paper presented at: Specialized Collections2015.

125. Mensing JP, Kerdcharoen T, Sriprachuabwong C, et al. Facile preparation of graphene–metal phthalocyanine hybrid material by electrolytic exfoliation. *Journal of Materials Chemistry*. 2012;22(33):17094-17099.

126. Kuila T, Khanra P, Kim NH, Choi SK, Yun HJ, Lee JH. One-step electrochemical synthesis of 6-amino-4-hydroxy-2-napthalene-sulfonic acid functionalized graphene for green energy storage electrode materials. *Nanotechnology*. 2013;24(36):365706.

127. Paredes JI, Munuera J. Recent advances and energy-related applications of high quality/chemically doped graphenes obtained by electrochemical exfoliation methods. *Journal of Materials Chemistry A.* 2017;5(16):7228-7242.

128. Rao KS, Sentilnathan J, Cho HW, Wu JJ, Yoshimura M. Soft Processing of Graphene Nanosheets by Glycine-Bisulfate Ionic-Complex-Assisted Electrochemical Exfoliation of Graphite for Reduction Catalysis. *Advanced Functional Materials.* 2015;25(2):298-305.

129. Chen C-H, Yang S-W, Chuang M-C, Woon W-Y, Su C-Y. Towards the continuous production of high crystallinity graphene via electrochemical exfoliation with molecular in situ encapsulation. *Nanoscale.* 2015;7(37):15362-15373.

130. Hossain ST, Wang R. Electrochemical Exfoliation of Graphite: Effect of Temperature and Hydrogen Peroxide Addition. *Electrochimica Acta.* 2016;216:253-260.

131. Yang S, Brüller S, Wu Z-S, et al. Organic radical-assisted electrochemical exfoliation for the scalable production of high-quality graphene. *J. Am. Chem. Soc*. 2015;137(43):13927-13932.

132. Zhong YL, Swager TM. Enhanced electrochemical expansion of graphite for in situ electrochemical functionalization. *Journal of the American Chemical Society*. 2012;134(43):17896-17899.

133. Liscio A, Kouroupis-Agalou K, Betriu XD, et al. Evolution of the size and shape of 2D nanosheets during ultrasonic fragmentation. *2D Materials.* 2017;4(2):025017.

134. Salavagione H, Sherwood J, Budarin V, Ellis G, Clark J, Shuttleworth P. Identification of high performance solvents for the sustainable processing of graphene. *Green Chemistry*. 2017;19(11):2550-2560.

135. Brennen C. Fundamentals of Multiphase flows. 2005 California. Cambridge University Press.

136. Cullen PL, Cox KM, Subhan MKB, et al. Ionic solutions of two-dimensional materials. *Nature Chemistry*. 2017;9(3):244-249.

137. Britnell L, Ribeiro R, Eckmann A, et al. Strong light-matter interactions in heterostructures of atomically thin films. *Science*. 2013;340(6138):1311-1314.

138. Wu Q, Jang SK, Park S, et al. In situ synthesis of a large area boron nitride/graphene monolayer/boron nitride film by chemical vapor deposition. *Nanoscale*. 2015;7(17):7574-7579.

139. Novoselov K, Mishchenko A, Carvalho A, Neto AC. 2D materials and van der Waals heterostructures. *Science*. 2016;353(6298):aac9439.

140. Herron CR, Coleman KS, Edwards RS, Mendis BG. Simple and scalable route for the 'bottom-up'synthesis of few-layer graphene platelets and thin films. *Journal of Materials Chemistry*. 2011;21(10):3378-3383.

141. Wang S, Hibino H, Suzuki S, Yamamoto H. Atmospheric pressure chemical vapor deposition growth of millimeter-scale single-crystalline graphene on the copper surface with a native oxide layer. *Chemistry of Materials*. 2016;28(14):4893-4900.

142. Bointon TH, Barnes MD, Russo S, Craciun MF. High Quality Monolayer Graphene Synthesized by Resistive Heating Cold Wall Chemical Vapor Deposition. *Advanced Materials*. 2015;27(28):4200-4206.

143. Polsen ES, McNerny DQ, Viswanath B, Pattinson SW, Hart AJ. High-speed roll-to-roll manufacturing of graphene using a concentric tube CVD reactor. *Scientific reports*. 2015;5.

144. Subrahmanyam K, Panchakarla L, Govindaraj A, Rao C. Simple method of preparing graphene flakes by an arc-discharge method. *The Journal of Physical Chemistry C*. 2009;113(11):4257-4259.

145. Qin B, Zhang T, Chen H, Ma Y. The growth mechanism of few-layer graphene in the arc discharge process. *Carbon*. 2016;102:494-498.

146. Chen Y, Zhao H, Sheng L, et al. Mass-production of highly-crystalline few-layer graphene sheets by arc discharge in various H 2–inert gas mixtures. *Chemical Physics Letters.* 2012;538:72-76.

147. Kruskopf M, Pakdehi DM, Pierz K, et al. Comeback of epitaxial graphene for electronics: large-area growth of bilayer-free graphene on SiC. *2D Materials.* 2016;3(4):041002.

148. Green AA, Hersam MC. Solution phase production of graphene with controlled thickness via density differentiation. *Nano Letters.* 2009;9(12):4031-4036.

149. Choi E-Y, San Choi W, Lee YB, Noh Y-Y. Production of graphene by exfoliation of graphite in a volatile organic solvent. *Nanotechnology.* 2011;22(36):365601.

150. Oh SY, Kim SH, Chi YS, Kang TJ. Fabrication of oxide-free graphene suspension and transparent thin films using amide solvent and thermal treatment. *Applied Surface Science.* 2012;258(22):8837-8844.

151. Ghislandi M, Tkalya E, Schillinger S, Koning CE, de With G. High performance graphene- and MWCNTs-based PS/PPO composites obtained via organic solvent dispersion. *Composites Science and Technology.* 2013;80:16-22.

152. Hasan T, Torrisi F, Sun Z, et al. Solution-phase exfoliation of graphite for ultrafast photonics. *physica status solidi (b).* 2010;247(11-12):2953-2957.

153. Chabot V, Kim B, Sloper B, Tzoganakis C, Yu A. High yield production and purification of few layer graphene by gum arabic assisted physical sonication. *Scientific reports.* 2013;3.

154. Kang MS, Kim KT, Lee JU, Jo WH. Direct exfoliation of graphite using a non-ionic polymer surfactant for fabrication of transparent and conductive graphene films. *Journal of Materials Chemistry C.* 2013;1(9):1870-1875.

155. Jayasena B, Subbiah S. A novel mechanical cleavage method for synthesizing few-layer graphenes. *Nanoscale Res. Lett.* 2011;6(1):95-101.

156. Zhao W, Fang M, Wu F, Wu H, Wang L, Chen G. Preparation of graphene by exfoliation of graphite using wet ball milling. *J. Mater. Chem.* 2010;20(28):5817-5819.

157. Aparna R, Sivakumar N, Balakrishnan A, Nair AS, Nair SV, Subramanian K. An effective route to produce few-layer graphene using combinatorial ball milling and strong aqueous exfoliants. *Journal of Renewable and Sustainable Energy*. 2013;5(3):033123.

158. Lin T, Tang Y, Wang Y, et al. Scotch-tape-like exfoliation of graphite assisted with elemental sulfur and graphene–sulfur composites for high-performance lithium-sulfur batteries. *Energy & Environmental Science*. 2013;6(4):1283-1290.

159. Jeon I-Y, Shin Y-R, Sohn G-J, et al. Edge-carboxylated graphene nanosheets via ball milling. *Proceedings of the National Academy of Sciences*. 2012;109(15):5588-5593.

160. Moon IK, Lee J, Ruoff RS, Lee H. Reduced graphene oxide by chemical graphitization. *Nature communications*. 2010;1:73.

161. Feng H, Cheng R, Zhao X, Duan X, Li J. A low-temperature method to produce highly reduced graphene oxide. *Nature communications*. 2013;4:1539.

162. Schniepp HC, Li J-L, McAllister MJ, et al. Functionalized single graphene sheets derived from splitting graphite oxide. *The Journal of Physical Chemistry B*. 2006;110(17):8535-8539.

163. Liao K-H, Mittal A, Bose S, Leighton C, Mkhoyan KA, Macosko CW. Aqueous only route toward graphene from graphite oxide. *ACS nano*. 2011;5(2):1253-1258.

164. Voiry D, Yang J, Kupferberg J, et al. High-quality graphene via microwave reduction of solution-exfoliated graphene oxide. *Science*. 2016;353(6306):1413-1416.

165. Dimiev AM, Tour JM. Mechanism of graphene oxide formation. *ACS nano*. 2014;8(3):3060-3068.

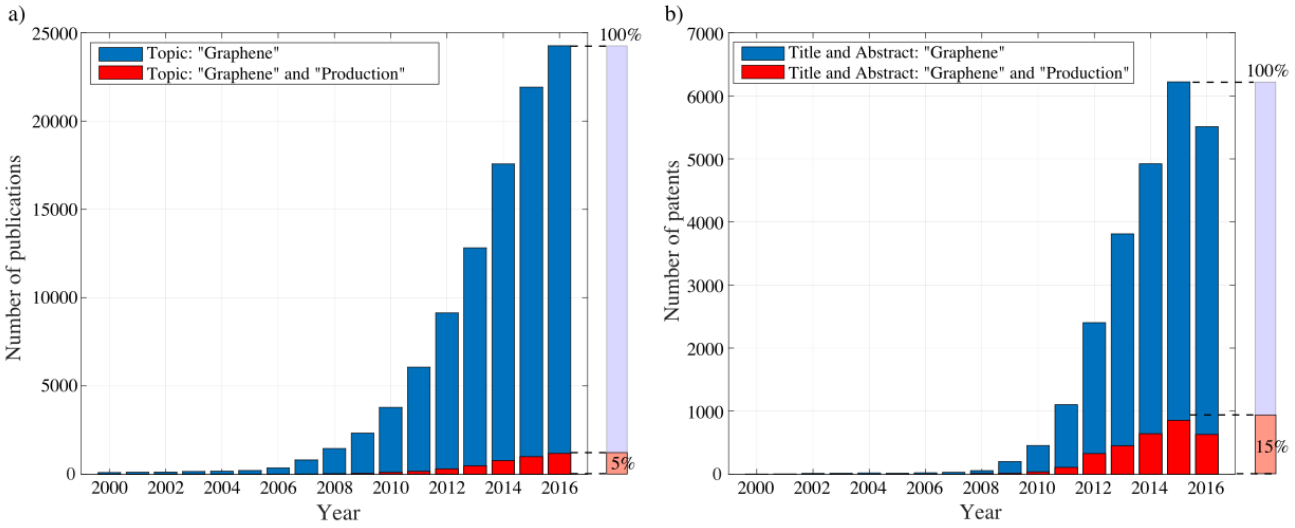

Figure 1: Publications and Patents in the field of graphene and graphene production. a) Number of publications on Graphene and Graphene Production from 2000 to 2016. This information was sourced from ISI Web of science. Search criteria for both are: Topic= "Graphene" and Topic= "Graphene" and "Production" respectively. b) Number of patents on Graphene and Graphene production from 2000 to 2016. This information was sourced through a worldwide search using the European Patent Offices Espacenet database. Search criteria for both are: Title and Abstract= "Graphene" and Title and Abstract= "Graphene" and "Production" respectively. Data for 2016 is incomplete and lower than expected as there is a typical timeline between filing and publication.

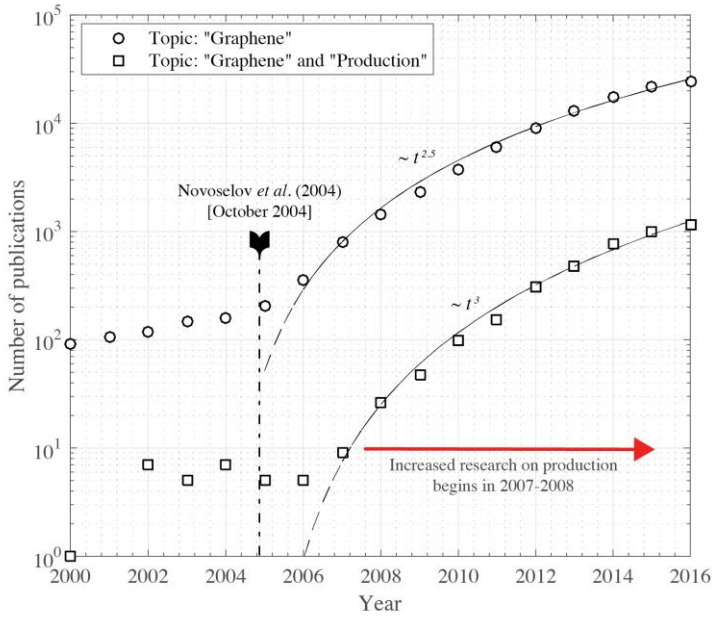

Figure 2: The trends in number of publications for Graphene and Graphene Production topics between 2000 and 2016. Data taken from Figure 1 a).

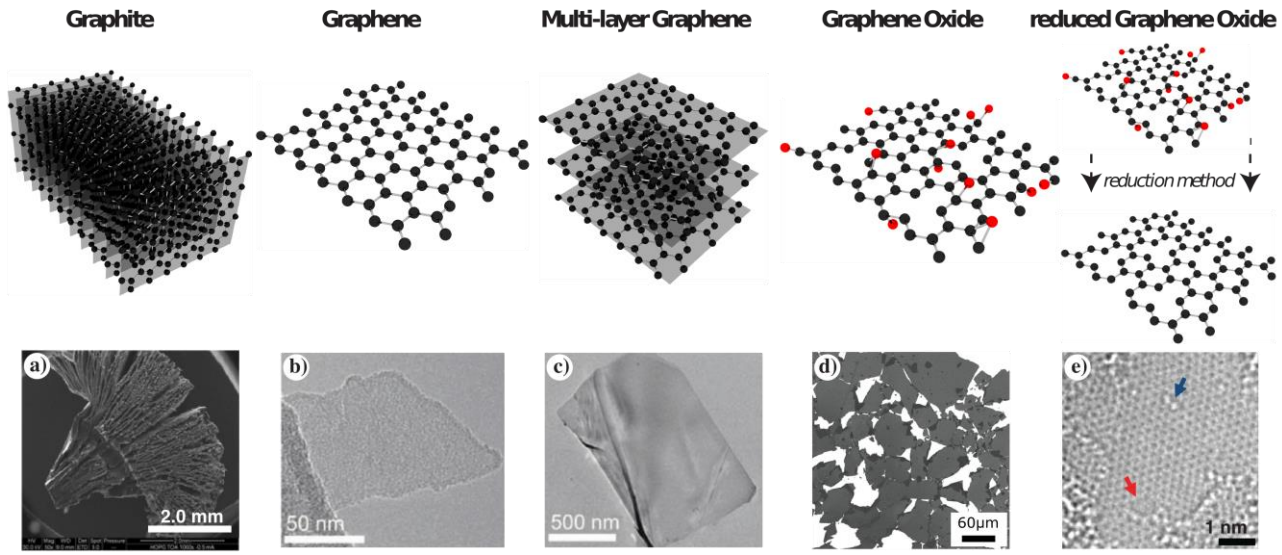

Figure 3: Overview of graphite and the various types of graphene-based materials with corresponding representative microscopy images. a) Scanning Electron Microscopy (SEM) image of expanded highly orientated pyrolytic graphite from Cooper *et al.* (b - c) TEM images of mono- and multi-layer graphene from Qian *et al.* d) SEM image of GO from Voiry *et al.* e) High resolution TEM (HRTEM) image of single layer reduced graphene oxide with indications of holes (red arrow) and oxygen functional groups (blue arrow) from Voiry *et al.* Reproduced with permission from ref. [53], [26] and [164]. Copyright 2014 Elsevier B.V., Copyright 2009 Springer, Copyright 2016 American Association for the Advancement of Science.

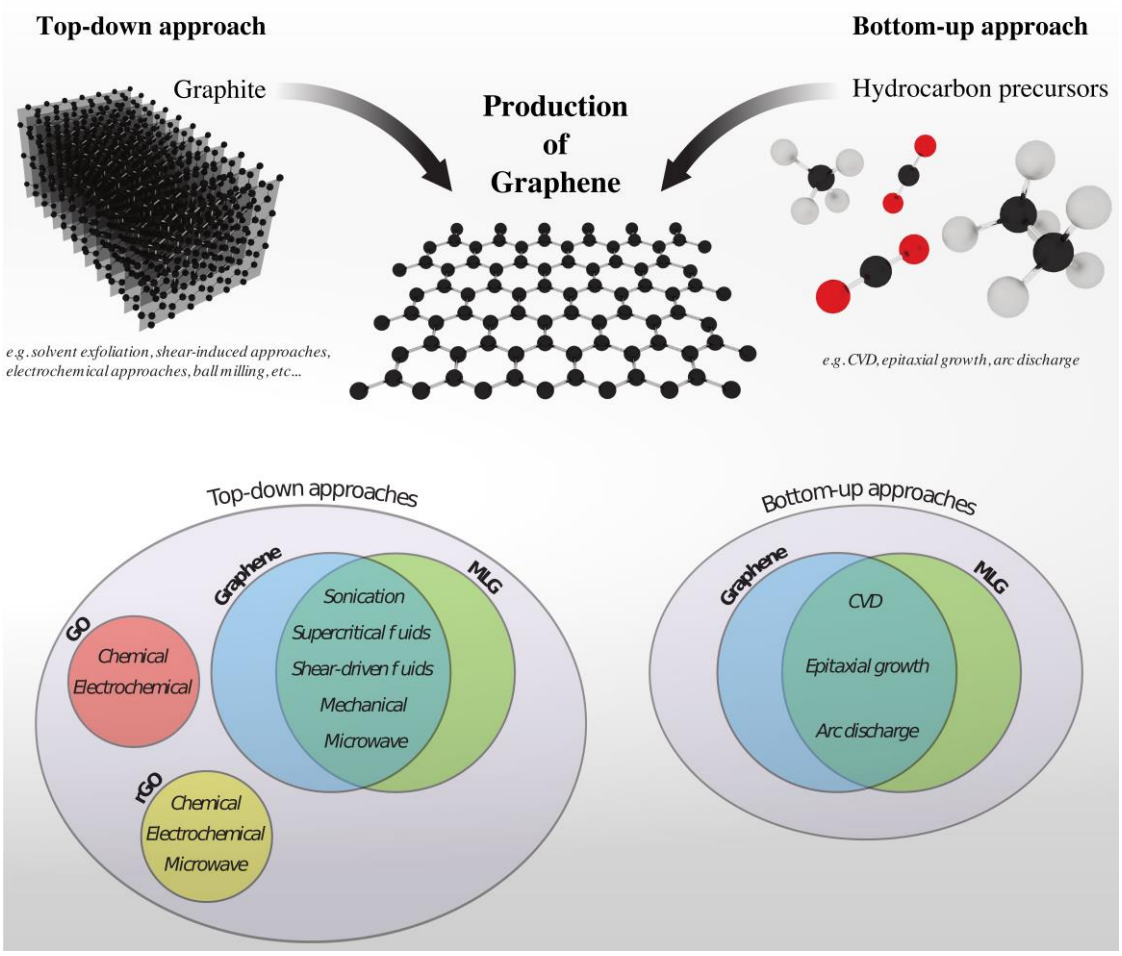

Figure 4: Top-down and bottom-up routes to graphene production. The intrinsic relationship between production (also reduction) approaches and graphene-based material type is also shown.

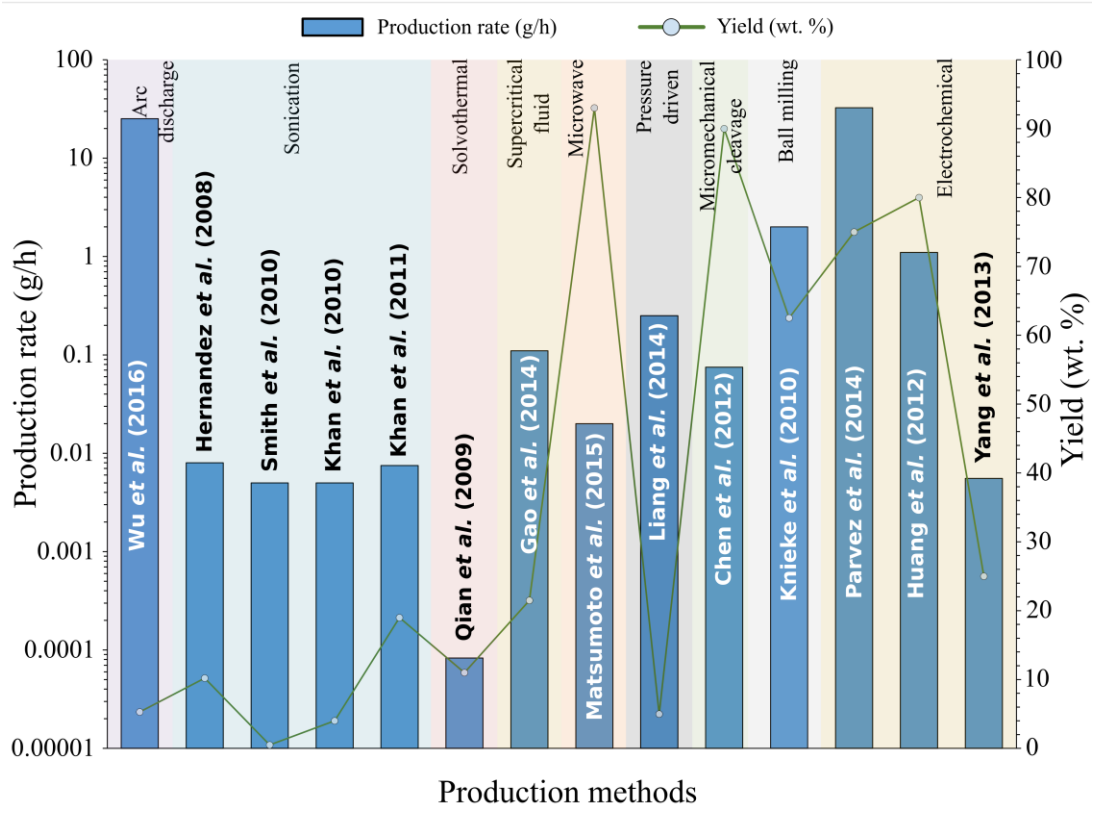

Figure 5: Summary of graphene production methods [16-29] . Criteria for data selection: a method results in at least 50% production of graphene with ≤5 layers, and has reported values for yield (wt%) and production rate (g/h).

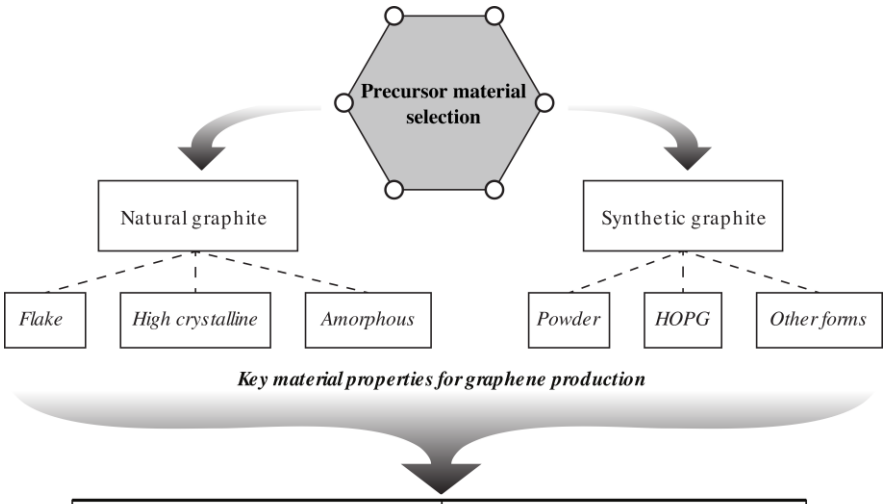

Graphite properties	Effects on production metrics
Particle lateral size and thickness	Degree of exfoliation and yield towards graphene monolayer
Morphology, bulk density and latice defects	Graphene's unique properties and functionalities, exfoliation efficiency, and maximum dispersion concentration
Purity (carbon content, C/O ratio, pH, moisture and sulfur %, other impurities e.g. metal)	Exfoliation efficiency, graphene purity and target application of graphene product

Figure 6: Summary of the graphite precursor considerations and effects on graphene production.

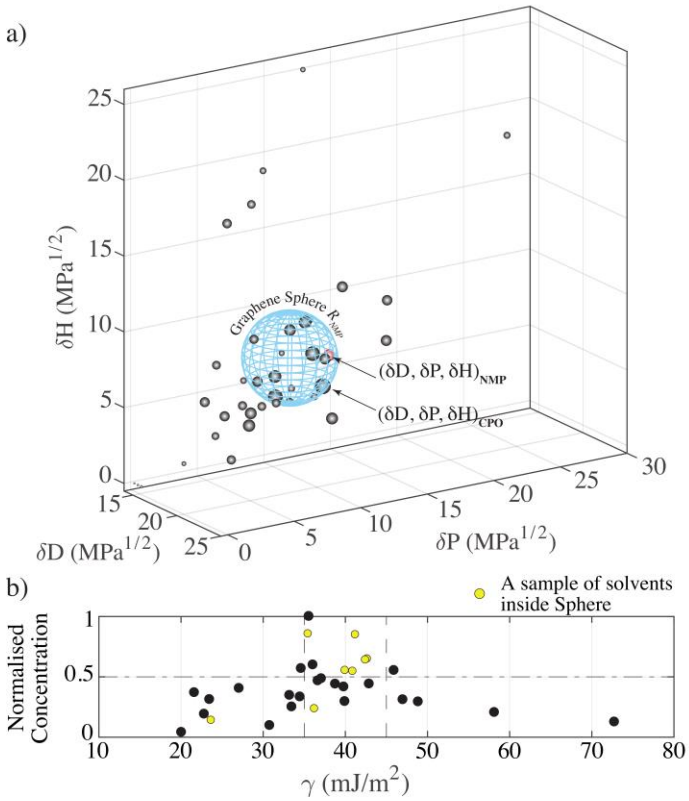

Figure 7: a) Hansen space representation and b) surface tension plot of solvents used for exfoliation and dispersion of graphene. Experimental data from [62].

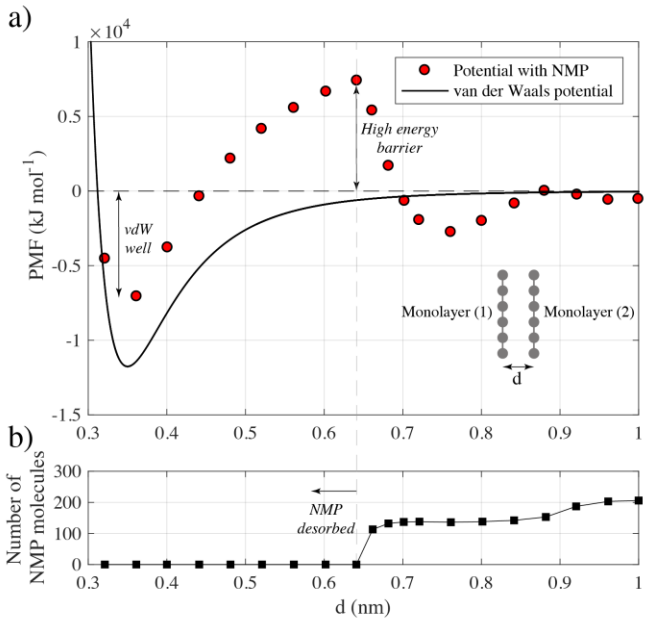

Figure 8: a) Comparison between the potential of mean force for NMP, predicted by MD simulations of two graphene monolayers [66], and the classical Lennard-Jones (van der Waals) interaction potential in vacuum. b) The number of NMP molecules confined between the two graphene monolayers [66].

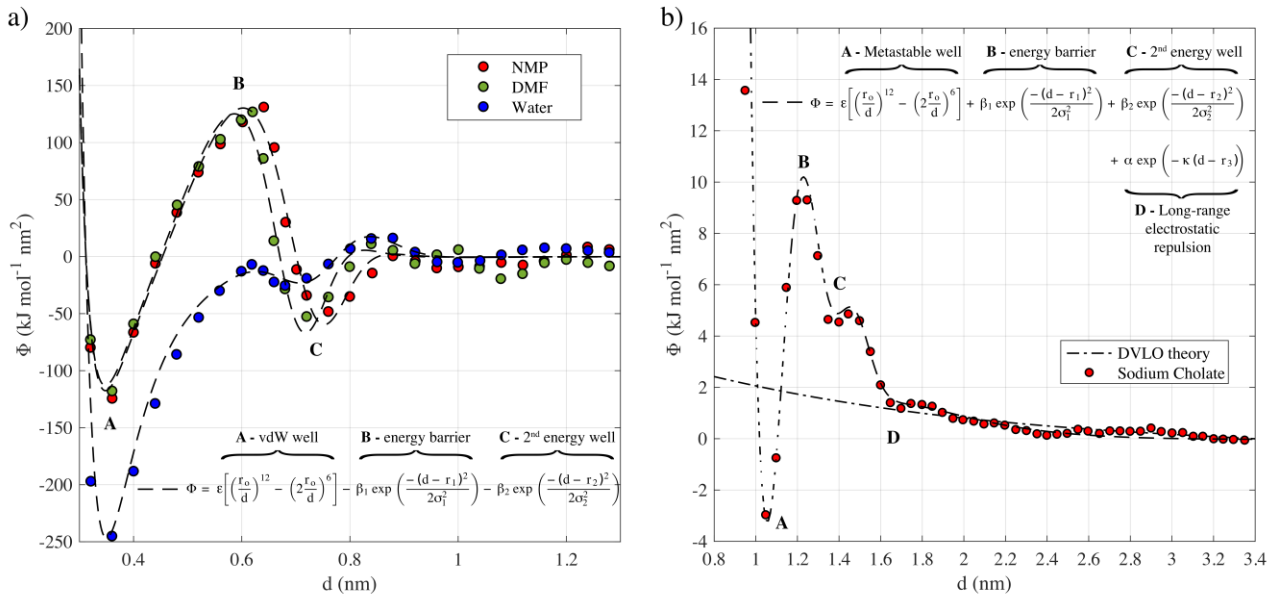

Figure 9: Interaction potentials, represented by the potential of mean force per unit area, between two graphene sheets in a) NMP, DMF and Water, and b) in an aqueous surfactant solution using Sodium Cholate (SC). Data points are MD simulation data from [66] and [71].

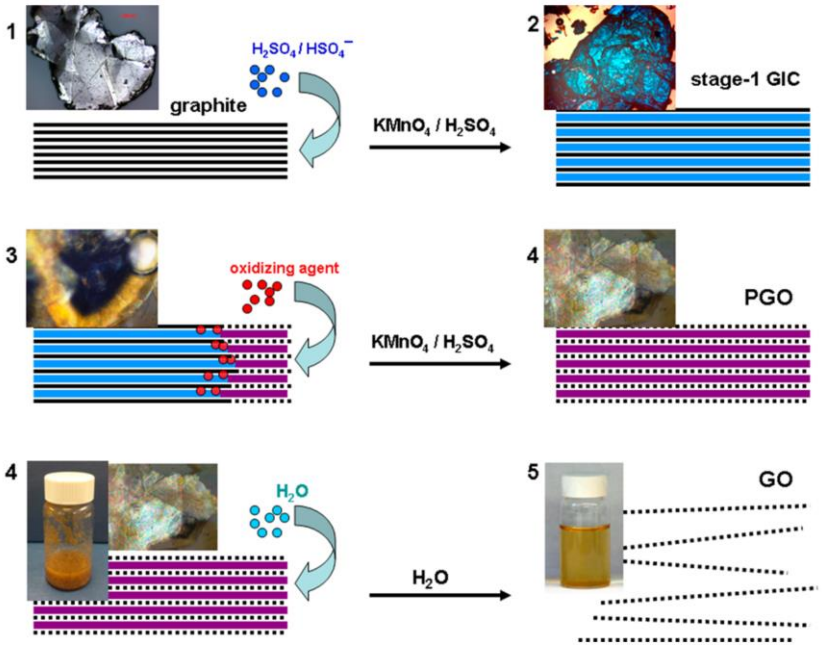

Figure 10: Schematics of the conversion of bulk graphite into graphene oxide with corresponding micrographic images or sample appearances at each phase. The three steps indicate the formation of the two intermediate products (graphite intercalated compound, GIC, and pristine graphite oxide (PGO)) and the final GO product. The solid black lines represent graphene layers; dotted black lines represent single layers of GO; wide blue lines represent H_2SO_4/HSO_4^- intercalant; wide purple lines represent a layer of the mixture of H_2SO_4/HSO_4^- intercalant with the reduced form of oxidizing agent. Reproduced with permission from ref.[165]. Copyright 2014 American Chemical Society.

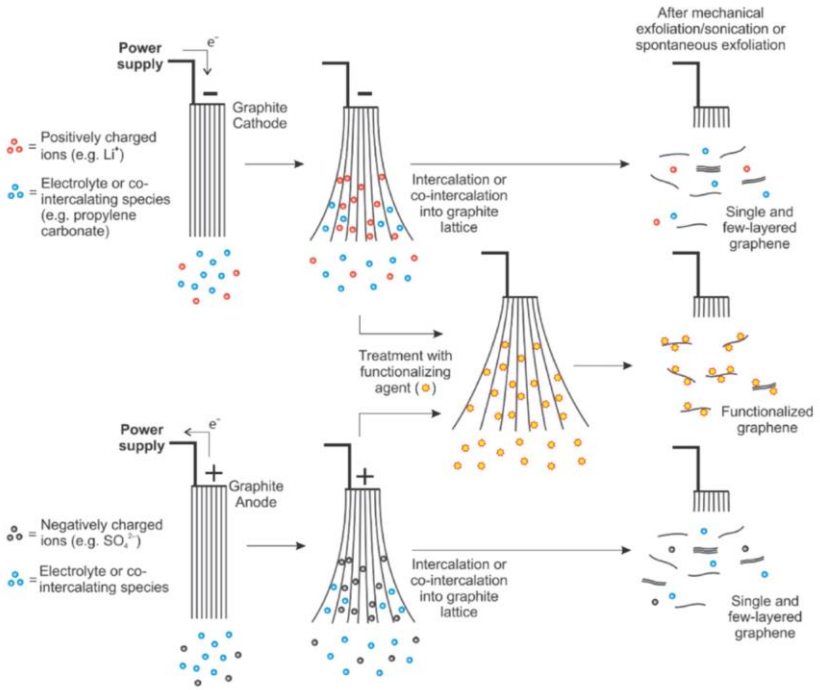

Figure 11: Schematic overview of cathodic and anodic exfoliation mechanisms. A positive or negative charge is created at a graphite working electrode, attracting oppositely charged intercalating ions. Reproduced with permission from ref. [93]. Copyright 2015 Elsevier B.V.

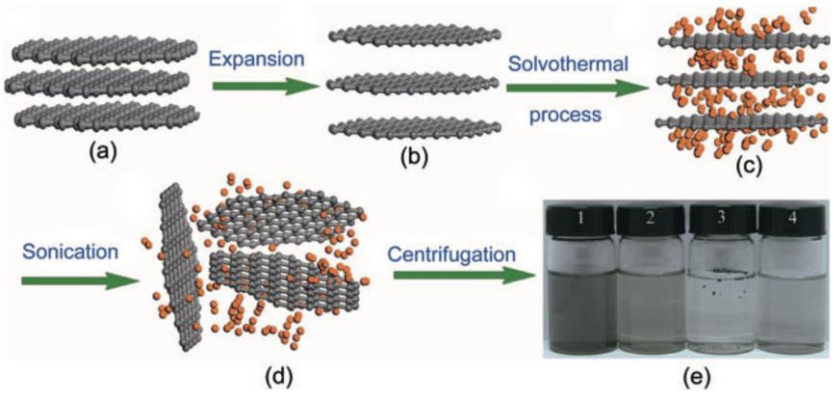

Figure 12: Schematic illustration of solvothermal-assisted exfoliation and dispersion of graphene sheets in acetonitrile: a) pristine expandable graphite. b) expanded graphite. c) schematic showing the insertion of acetinitrile molecules into the interlayers of expanded graphite. d) exfoliated graphene sheets dispersed in acetonitrile. e) optical images of four samples obtained under the different conditions described in Table 3. Reproduced with permission from ref. [26]. Copyright 2009 Tsinghua University Press and Springer Berlin Heidelberg.

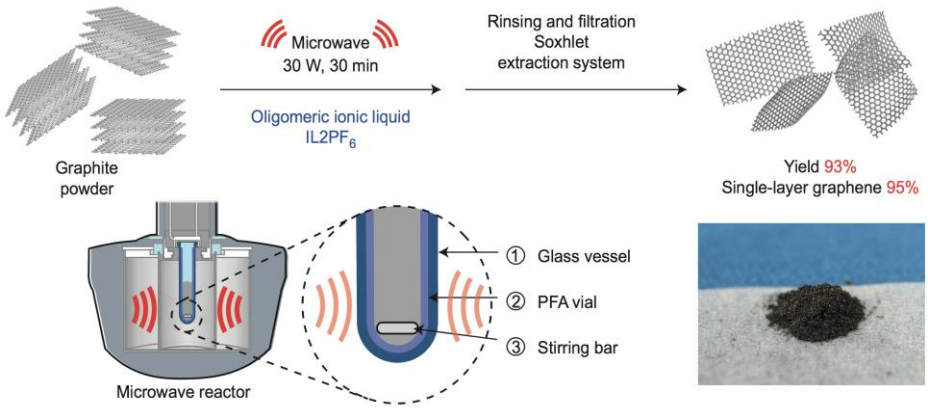

Figure 13: Overview of the microwave-assisted liquid-phase exfoliation of graphite in ionic liquids with a schematic of the 'reaction' set-up. Typically, a vial containing a graphite suspension in ionic liquid was placed in a glass reaction vessel. This vessel was then placed in a microwave reactor operating at 2.45 GHz and irradiated using a single-mode microwave setting at 30 W for 30 min. The microwave-irradiated mixture of graphite in ionic liquid was diluted with dimethylsulfoxide (DMSO), and the entire mixture was transferred to a PTFE thimble filter. The solid residue in the thimble filter was rinsed successively with DMSO (reduced pressure; ~30 mmHg), 2,2,2-trifluoroethanol and dichloromethane by using a Soxhlet extraction system, and subsequently dried under reduced pressure to create a black powder (bottom right) that contained 95% single-layer graphene (93% yield). Reproduced with permission from ref. [24]. Copyright 2015 Nature Publishing Group.

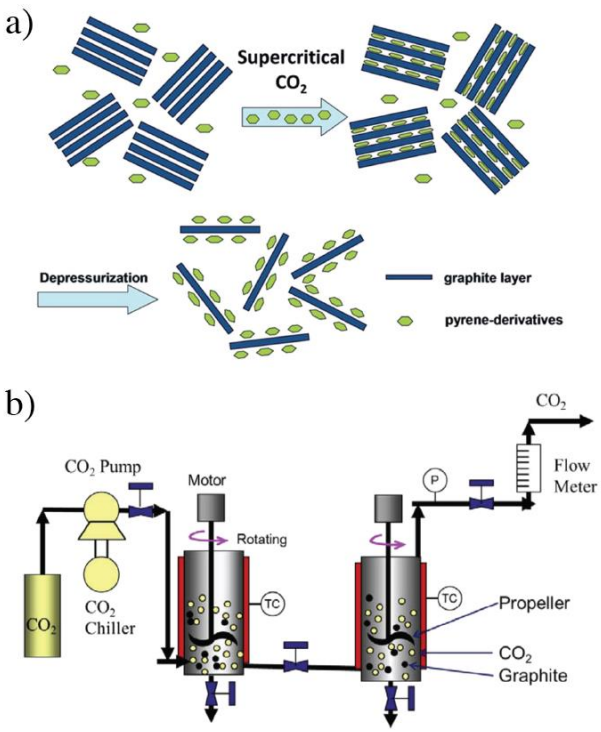

Figure 14: a) Schematic of the exfoliation of graphite using a supercritical fluid (i.e. CO_2). In this instance, graphene was simultaneously modified with pyrene-derivatives. b) Schematic of an experimental device to exfoliate graphite using a supercritical fluid. Reproduced with permission from ref. [43,84]. Copyright 2013 American Chemical Society, Copyright 2016 Elsevier.

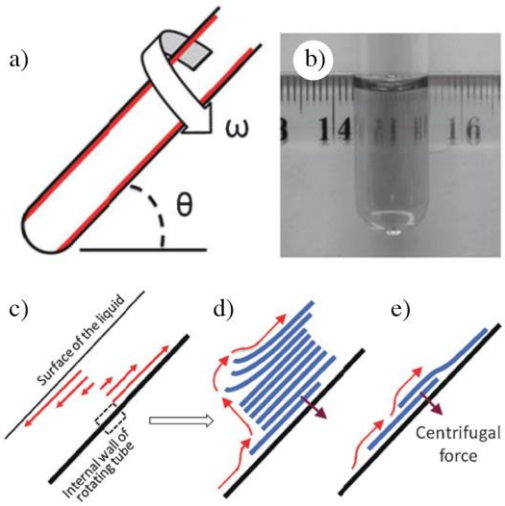

Figure 15: a) Schematic of the vortex fluidic device used to exfoliate graphite and boron nitride (10 mm diameter tube, 16 cm long, inclined at 45°, operating at 7000 and 8000 rpm for graphite and boron nitride, respectively). b) Photographs of the resulting colloidal suspensions of graphene (top) in NMP. Illustrations of c) the microfluidic flow velocity indicted by red arrows for a section of the rotating tube; d) the exfoliation process; and e) slippage on the inner surface of the tube. Reproduced with permission from ref. [104]. Copyright 2012 The Royal Society of Chemistry.

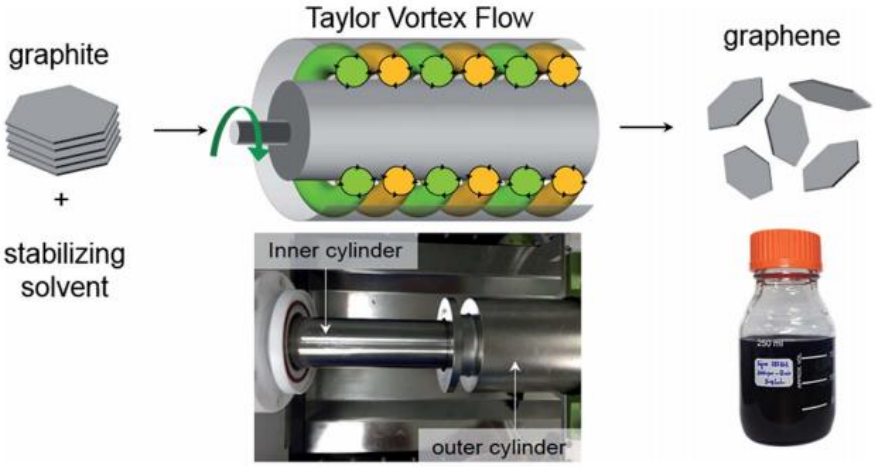

Figure 16: Schematic of the shear-exfoliation of graphite into few-layer graphene by a Taylor Vortex flow. Photographs shows a Taylor–Couette flow reactor and the graphene dispersions produced by shear exfoliation. The volume in the reactor for mixing was 200 mL, and the gap between the two concentric cylinders was 2.5 mm. Reproduced with permission from ref. [106]. Copyright 2016 The Royal Society of Chemistry.

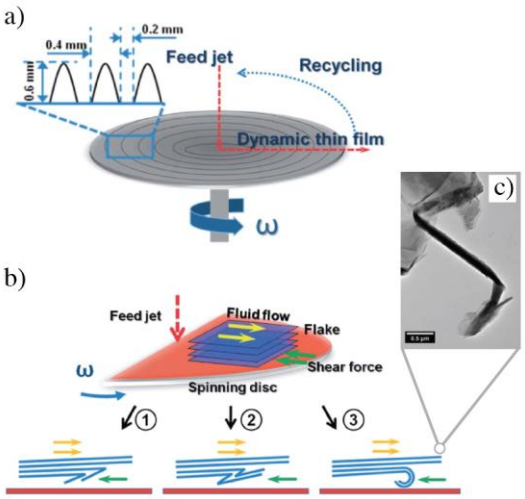

Figure 17: a) Schematic of the spinning disc processor used for exfoliation of graphite (20 cm diameter stainless steel disc operating at 2500 rpm). b) Proposed mechanism of exfoliation and scrolling of graphite and boron nitride flakes using the set-up. c) TEM image of partial carbon nanoscroll. Reproduced with permission from ref. [107]. Copyright 2012 The Royal Society of Chemistry.

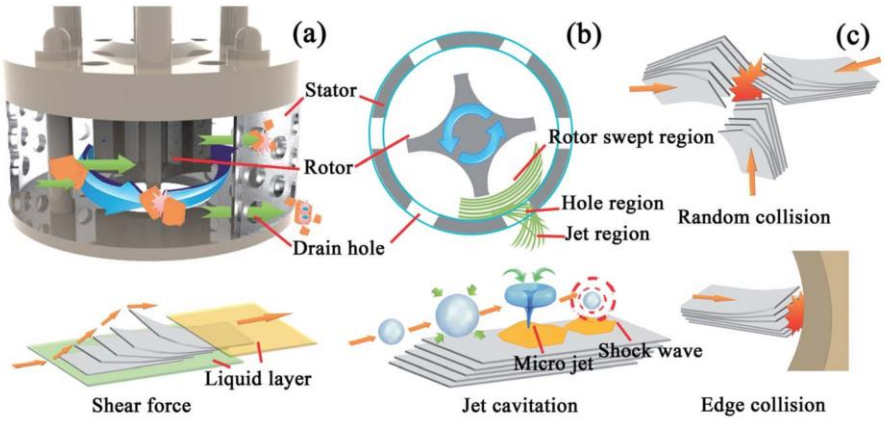

Figure 18: a) 3D sectional drawing of a high-shear mixer for the production of graphene. b) Main energy dissipation regions of the high-shear mixer (sectional view). c) Schematic of preparing graphene nanosheets by shear force, collision and jet cavitation. Reproduced with permission from ref. [41]. Copyright 2014 The Royal Society of Chemistry.

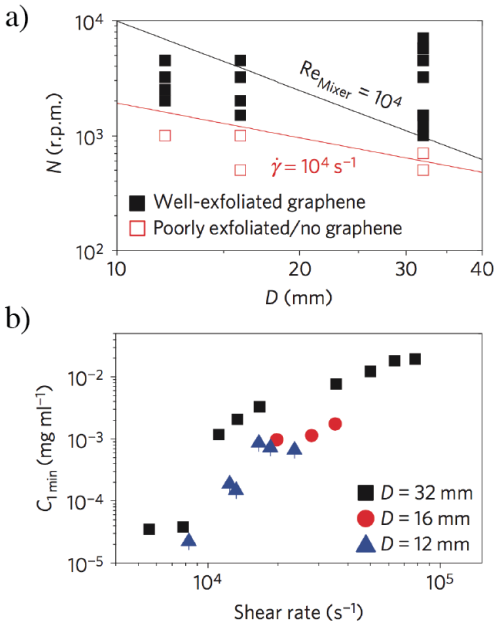

Figure 19: Overview of the outputs using a high shear mixing process for exfoliation. a) Phase diagram of rotor speed, N, versus diameter, D, for dispersions showing good exfoliation according to TEM. The region above the black line represents fully developed turbulence, that is, $Re_{Mixer} > 10^4$, whereas the region above the red line represents $\dot{\gamma}\,min > 10^4\ s^{-1}$. b) Concentration of graphene produced in the Silverson shear mixer as a function of shear rate for rotors with diameters of 32, 16 and 12 mm (mixing time 1 min). All three data sets are consistent with the same minimum shear rate. Reproduced with permission from ref. [40]. Copyright 2014 Nature Publishing Group.

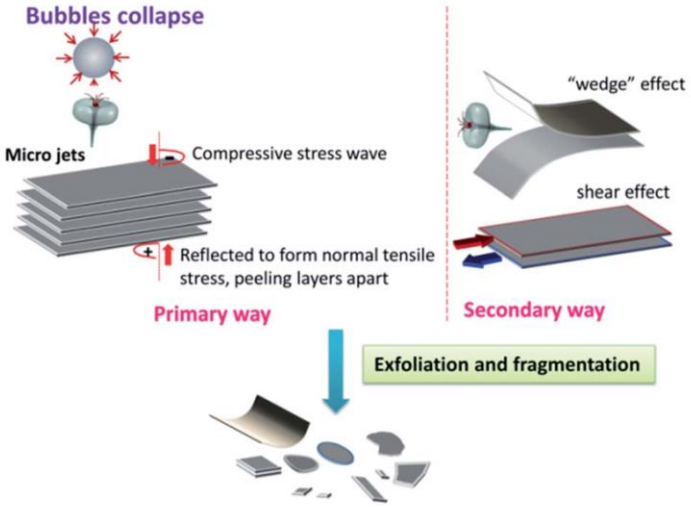

Figure 20: An illustration of the mechanical mechanism for exfoliation via sonication. Reproduced with permission from ref. [84]. Copyright 2015 The Royal Society of Chemistry.

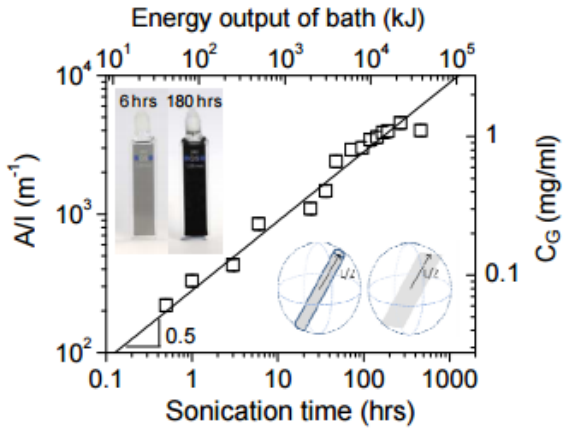

Figure 21: Concentration of graphene after centrifugation as a function of sonication time. On the left axis is the measured absorbance per cell length, A/l, while the right axis corresponds to the concentration calculated using an absorption coefficient of 3620 mL mg^{-1} m^{-1}. The upper axis shows the total energy outputted by the bath calculated using the measured power output of 23 W. Reproduced with permission from ref. [20]. Copyright 2010 John Wiley & Sons, Inc.

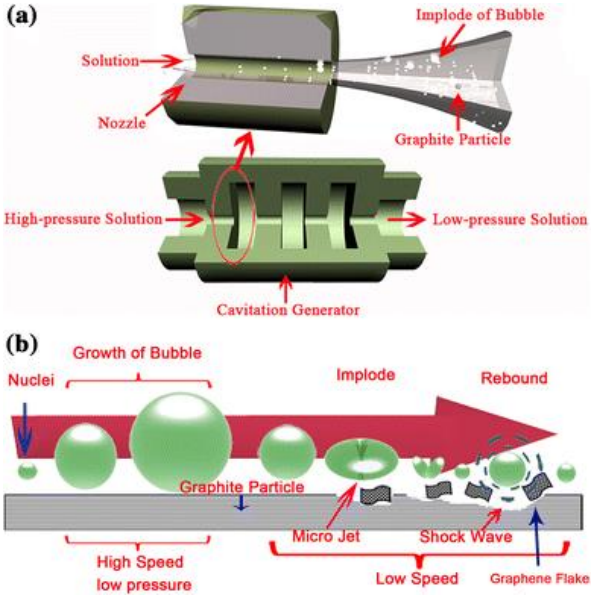

Figure 22: a) Schematic of the cavitation generator. b) Illustration of the mechanisms during the production of graphene flakes by jet cavitation. Reproduced with permission from ref. [119] . Copyright 2014 Springer.

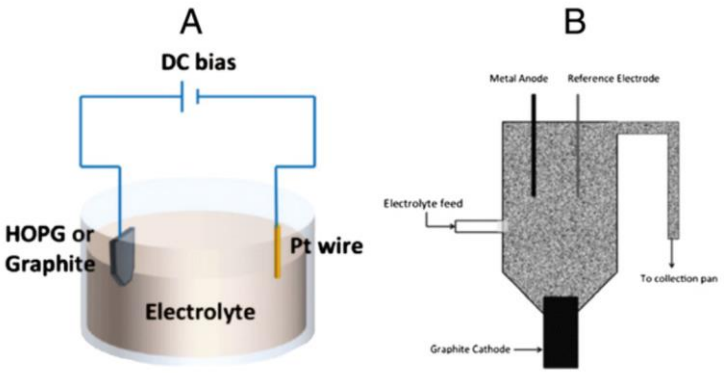

Figure 23: a) Schematic of a typical setup for the electrochemical exfoliation of graphite. b) A novel setup for continuous electrochemical exfoliation process. Reproduced with permission from ref. [93] and [122]. Copyright 2011 American Chemical Society, Copyright 2014 American Chemical Society.

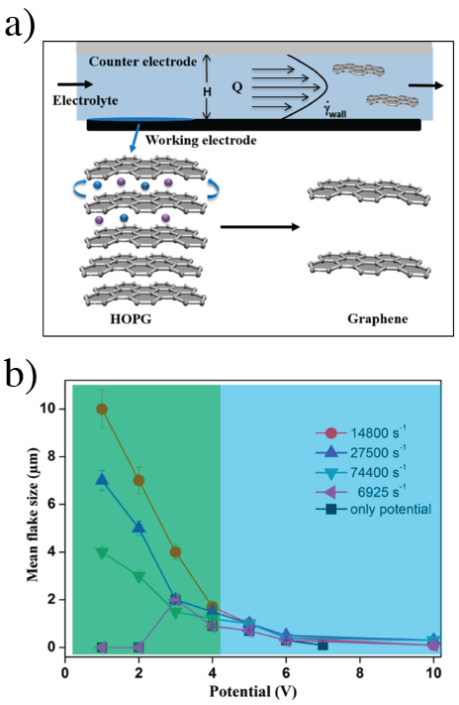

Figure 24: a) Schematic representation of the electrochemical micro-reactor combining electrochemical exfoliation and shear-driven exfoliation. The graphite crystal is both the wall and the working electrode of the reactor and simultaneously experiences a high wall shear rate and an applied electric potential. Here H, Q, and $\dot{\gamma}$ are the height between two electrodes, electrolyte flow, and shear rate, respectively [54]; b) Effect of potential and shear rate on the size of graphene flakes produced in the flow reactor. A mean size distribution of zero, specifically in the case for only potential and shear rate of 6925 s^{-1}, indicates that exfoliation was unnoticed over the samples that were measured. The green and blue colors in the figure indicate shear and potential dominated regions, respectively. Statistical flake size analysis for the graphene was performed using more than 80 sheets from AFM measurements. Error bars in these figures are from three samples at a given condition, showing the maximum and minimum values. Reproduced with permission from ref. [54]. Copyright 2016 American Chemical Society.

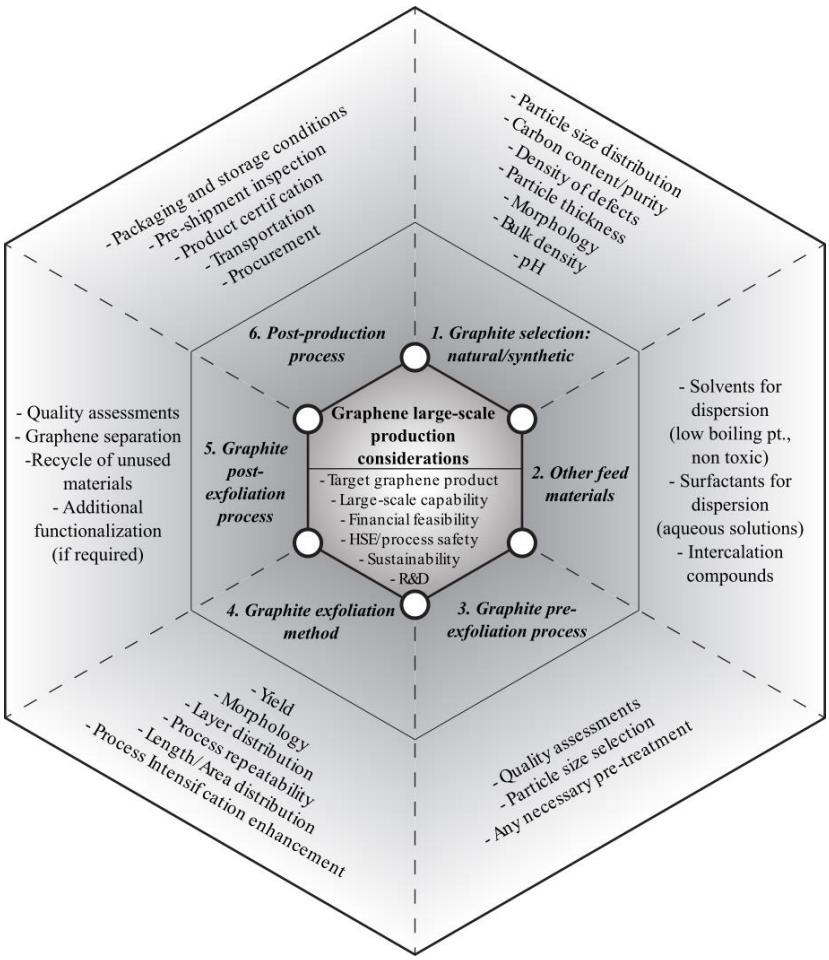

Figure 25: A summary of the top-down production considerations in the scale-up of graphene